

Tricyclic SpiroLactams Kill Mycobacteria In Vitro and In Vivo by Inhibiting Type II NADH Dehydrogenases

Sushovan Dam, Salia Tangara, Claire Hamela, Theo Hattabi, Léo Faïon, Paul Carre, Rudy Antoine, Adrien Herledan, Florence Leroux, Catherine Piveteau, Maxime Eveque, Marion Flipo, Benoit Deprez, Laurent Kremer, Nicolas Willand,* Baptiste Villemagne,* and Ruben C. Hartkoorn*



Cite This: *J. Med. Chem.* 2022, 65, 16651–16664



Read Online

ACCESS |



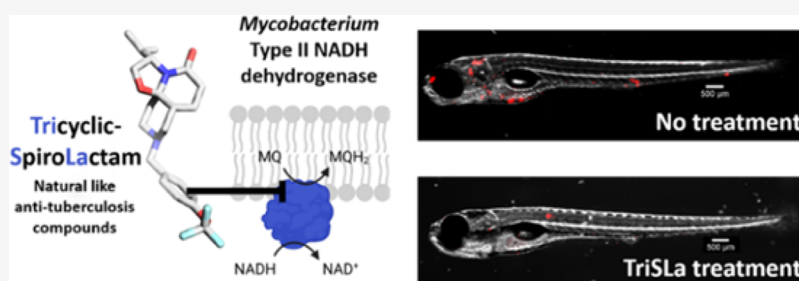
Metrics & More



Article Recommendations



Supporting Information



ABSTRACT: It is critical that novel classes of antituberculosis drugs are developed to combat the increasing burden of infections by multidrug-resistant strains. To identify such a novel class of antibiotics, a chemical library of unique 3-D bioinspired molecules was explored revealing a promising, mycobacterium specific Tricyclic SpiroLactam (TriSLa) hit. Chemical optimization of the TriSLa scaffold delivered potent analogues with nanomolar activity against replicating and nonreplicating *Mycobacterium tuberculosis*. Characterization of isolated TriSLa-resistant mutants, and biochemical studies, found TriSLas to act as allosteric inhibitors of type II NADH dehydrogenases (Ndh-2 of the electron transport chain), resulting in an increase in bacterial NADH/NAD⁺ ratios and decreased ATP levels. TriSLas are chemically distinct from other inhibitors of Ndh-2 but share a dependence for fatty acids for activity. Finally, in vivo proof-of-concept studies showed TriSLas to protect zebrafish larvae from *Mycobacterium marinum* infection, suggesting a vulnerability of Ndh-2 inhibition in mycobacterial infections.

INTRODUCTION

While global efforts to eradicate tuberculosis (TB) by improving drug access and treatment compliance have decreased deaths by 29% over the last two decades, TB remains the leading cause of death by an infectious disease worldwide.¹ With a minimum of 6 months of multidrug therapy, current TB treatment is notoriously lengthy, a feature largely attributed to the difficulty in eliminating phenotypically drug-tolerant subpopulations of the causative bacteria *Mycobacterium tuberculosis* (*Mtb*).² However, escalating infections by multidrug-resistant TB infections (483,000 cases of rifampicin-resistant TB reported in 2020¹) as well as extensively drug resistant (XDR) TB (12,350 cases reported in 2019³) require even longer therapy with less efficient and tolerated second-line drugs. In recognition of this global health problem, the World Health Organization has placed TB at the highest critical global priority of antibiotic-resistant bacteria for the development of new antibiotics.⁴

Concerted efforts to propose alternative and better antibiotics against drug-sensitive and -resistant TB have led to the approval of two novel classes of anti-TB drugs, the ATP synthase inhibitor bedaquiline,⁵ and the two nitroimidazole

prodrugs, delamanid⁶ and pretomanid.⁷ Additional anti-TB molecules are at various levels of clinical and preclinical drug development that may feed our treatment options in the future.^{8–10} Despite these increased efforts, it is clear that the TB drug development pipeline requires further supplementation with additional candidates, ideally acting on novel targets (to minimize cross-resistance) and impacting on drug-tolerant bacilli to shorten the duration of the treatment.

For the discovery of novel anti-TB drugs, phenotypic screening of chemical libraries on whole bacteria has proven to be the most successful approach.¹¹ The vast majority of synthetic molecules screened against *Mtb*, and hence emerged as leads, are largely flat (two-dimensional) in structure and comprise many sp²-rich aromatic cores.¹² Such flat molecules are in stark contrast to the often complex three-dimensional

Received: September 10, 2022

Published: December 6, 2022



(3D) structures of natural products, historically representing an important source of antibiotics. The molecular shape of such biomolecules plays a key role in their interaction with protein targets.¹³ Interestingly, the *Mtb* ATP synthase inhibitor bedaquiline buckles this trend as an antibiotic of synthetic origin, being highly 3D in shape, thanks to the two central adjacent highly substituted sp³-hybridized carbon atoms. With the rationale that molecules with increased 3D structures will allow for the probing of previously unexplored chemical and biological space, a “natural-like” chemical library with sp³-rich synthetic molecules was assembled^{14–19} and evaluated for anti-TB activity.^{20,21}

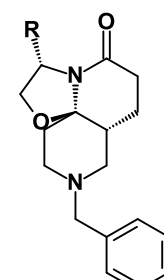
Herein, we show that the screening of chemical libraries with increased 3D diversity can result in the identification of novel chemical- and biological-space to combat *Mtb*. This work describes the identification of the Tricyclic SpiroLactam (TriSLa) chemical family and its chemical optimization to potent nanomolar antimycobacterial compounds with particular activity against *Mtb*. Target identification and validation studies revealed that TriSLas act through the inhibition of the mycobacterial type II NADH dehydrogenase. TriSLas exhibited a time-dependent bactericidal activity on *Mtb* and was also active on nonreplicating and intracellular bacilli. Subsequent in vivo efficacy studies of TriSLas on *Mycobacterium marinum*-infected zebrafish larvae confirmed efficacy and validated type-2 NADH dehydrogenase as a vulnerable and druggable target in mycobacteria.

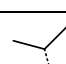
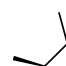
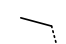
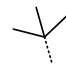

RESULTS

Discovery of TriSLa Antituberculosis Lead Compounds. With the aim of investigating the anti-TB potential of new chemical spaces, we assembled a focused chemical library of 958 in-house synthetic “natural-like” compounds. These molecules display enhanced 3D properties, a high number of sp³-hybridized carbon atoms (≥ 12), a calculated molecular complexity²² greater than 0.76, and a molecular shape index lower than 0.56, reflecting a greater sphericity (as measured using DataWarrior²³) (Figure S1a). Screening of this chemical library at 10 μM on replicating *Mtb* strain H37Rv led to the identification of compounds **1** and **2** (Table 1), two tricyclic spiroLactam analogues that inhibited bacterial growth. Following *de novo* re-synthesis and purification of these hits, **1** and **2** were confirmed to have a minimal inhibitory concentration (MIC) against *Mtb* of 3.2 and 9.5 μM respectively (as measured using the resazurin reduction assay). The more potent analogue **1** is a small lead-like molecule (low molecular weight of 328 g mol⁻¹, Lipinski and Veber rules compliant) with a high aqueous solubility (178 μM at pH 7.4) because of the basic nitrogen of the piperidine ring and favorable logD (2.7). The configuration of the stereogenic centers of **1** was confirmed by crystallization and X-ray diffraction of its hydrochloride salt (Figure S1c). To confirm the importance of the TriSLa configuration, compound **1**'s enantiomer (compound **3**, Figure S1b) was synthesized and found to be inactive against *Mtb* (MIC of 100 μM), supporting the hypothesis that the antibiotic activity is mediated by an interaction with a specific mycobacterial protein.

Hit-to-Lead Optimization: Medicinal Chemistry. Compound **1** represented an attractive starting point for the development of a new anti-TB chemotype, though its potency required improvement. Because replacement of the isopropyl moiety by a *sec*-butyl (compound **2**) was found to affect potency, we decided to explore other modifications in this

Table 1. Biological Activities of Compounds 1–7



compound	R	anti-TB activity MIC ₉₈ (range) (μM) ^a
1		3.2 (1.6-6.3)
2		9.5 (6.3-12.5)
4	H ₃ C	>100
5		18.8 (12.5-25)
6		25.0
7		37.5 (25-50)

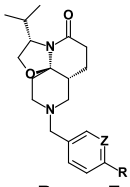
^aAnti-TB activity was determined on H37Rv grown in Middlebrook 7H9 media supplemented with 0.2% glycerol, 0.05% tween 80, and 10% OADC. MIC₉₈ represents the lowest concentration of compounds that prevented 98% of resazurin turnover by H37Rv compared to the untreated bacteria.

position (Table 1). Replacement of the isopropyl with smaller alkyl substituents (a methyl for compound **4** and an ethyl for compound **5**) led to a loss of activity (MIC > 100 μM and MIC = 18.8 μM , respectively). A similar result was obtained with a larger *tert*-butyl moiety (compound **6**, MIC = 25 μM). Introduction of a cyclopropyl (compound **7**, MIC = 37.5 μM) also led to a 1-log decrease in potency.

Overall, these structure–activity relationships (SARs) suggested that the isopropyl moiety of compound **1** cannot be advantageously replaced. In parallel, metabolic stability studies of compound **1** showed high clearance (Table S1) largely because of hydroxylation of the benzyl moiety (Figure S2). For these reasons, modifications of the benzyl group were next prioritized in an attempt to both metabolically stabilize compound **1** and increase its antimicrobial potency.

The introduction of electron-donating groups such as methyl (compound **8**, MIC = 1.7 μM) or methoxy (compound **9**, MIC = 4.7 μM) in position 4 of the phenyl ring did not impact antibacterial potency (Table 2). On the other hand, introduction of an electron-withdrawing chlorine atom (compound **10**, MIC = 0.25 μM) led to a marked (>1-log) improvement in antibacterial potency. This effect was even more pronounced using a trifluoromethyl (compound **11**, MIC = 0.10 μM) or trifluoromethoxy (compound **12**, MIC = 0.13

Table 2. Summary of TriSLa Antituberculosis Activity, Biochemical Ndh-2 Inhibition, and Physicochemical Properties

Compound		R	Z	Anti-TB activity	Inhibition of <i>Mtb</i> MBP-Ndh		Inhibition of <i>Mtb</i> MBP-NdhA (from mc ² 155) ^[c] Mean IC ₅₀ ± SD (μM) n ≥ 5	Intra-cellular Mean IC ₅₀ ± SD (μM) ^[d]	Measured solubility in PBS (μM) ^[e]	PBS/Octanol partition coefficient LogD _{7.4} ^[f]
				MIC ₉₈ (Range) (μM) ^[a]	<i>E. coli</i> ^[b]	mc ² 155 ^[c]				
1	-H	CH	3.2 (1.6-6.3)	0.34 ± 0.09	0.47 ± 0.12	0.98 ± 0.25	8.2 ± 1.6	178	2.7	
8	-CH ₃	CH	1.7 (0.75-2.5)	ND	ND	ND	ND	ND	ND	
9	-OCH ₃	CH	4.7 (2.5-6.3)	0.20 ± 0.12	0.89 ± 0.25	2.34 ± 0.29	ND	ND	ND	
10	-Cl	CH	0.25 (0.16-0.31)	0.028 ± 0.011	0.042 ± 0.014	0.096 ± 0.026	ND	ND	ND	
(11, BDM88689)	-CF ₃	CH	0.10 (0.08-0.16)	0.012 ± 0.005	0.037 ± 0.025	0.059 ± 0.008	0.46 ± 0.11	148	3.4	
(12, BDM88690)	-OCF ₃	CH	0.13 (0.08-0.16)	0.012 ± 0.006	0.041 ± 0.017	0.057 ± 0.015	0.36 ± 0.03	133	3.9	
(13, BDM89000)	-CF ₃	N	0.59 (0.31-0.63)	0.032 ± 0.019	0.088 ± 0.027	0.33 ± 0.10	2.4 ± 1.3	>200	2.7	

^aAnti-TB activity was determined on H37Rv grown in Middlebrook 7H9 media supplemented with 0.2% glycerol, 0.05% tween 80, and 10% OADC. MIC₉₈ represents the lowest concentration of compounds that prevented 98% of resazurin turnover by H37Rv compared to the untreated bacteria. ^bBiochemical assays performed on recombinant MBP-Ndh purified from *E. coli*. ^cBiochemical assays performed on recombinant MBP-Ndh purified from *M. smegmatis* mc²155. ^dIntracellular activity of compounds was investigated by determining the concentration that protected 50% of the macrophages (IC₅₀) from a lethal H37Rv infection (MOI 10), with macrophage viability determined using the resazurin reduction assay. ^eSolubility measured in PBS pH 7.4 starting from a 10 mM solution in DMSO of the compound. ^flogD was measured at pH 7.4 between PBS and octanol. All compounds were tested at the same concentration (1 μM). n.d. not determined. MBP-Ndh stands for mannose binding protein-tagged Ndh.

Table 3. Spectrum of Antibiotic Activity of TriSLa Inhibitors^a

bacterial strain	MIC (μM)		
	compound 1	compound 11	compound 12
<i>M. tuberculosis</i> (H37Rv) ^b	3.2 (1.6–6.3)	0.10 (0.08–0.16)	0.13 (0.08–0.16)
<i>M. marinum</i> (M strain) ^b	6.3	0.19 (0.16–0.31)	0.16
<i>M. avium</i> (TMC 724, ATCC-25291) ^b	13.1 (3.1–25)	0.55 (0.16–1.25)	0.38 (0.16–0.63)
<i>M. smegmatis</i> (mc ² 155) ^b	29.2 (25–50)	1.3 (1.25–2.5)	1.3 (1.25–2.5)
<i>M. abscessus</i> (CIP104536, Smooth variant) ^b	≥100	5	8.1 (5–10)
<i>M. abscessus</i> (CIP104536, Rough variant) ^b	≥100	6.3 (5–10)	8.1 (5–10)
<i>Bacillus subtilis</i> (ATCC6633) ^c	>100	>100	>100
<i>Staphylococcus aureus</i> (SH1000) ^c	>100	>100	>100
<i>Escherichia coli</i> (BW25113) ^c	>100	>100	>100
<i>Escherichia coli</i> ΔtolC (BW25113 ΔtolC) ^c	>100	100	100
<i>Pseudomonas aeruginosa</i> (POA1) ^c	>100	>100	>100
<i>Klebsiella pneumoniae</i> (LMG 2095) ^c	>100	>100	>100
<i>Acinetobacter baumannii</i> (LMG-17978) ^c	>100	>100	>100

^aMIC values (in μM) were determined using the resazurin reduction assay, except for *M. marinum* and *P. aeruginosa* where viability was determined visually. Data are presented as an average MIC of at least three independent biological replicates with the range of MICs (where there was a range) indicated in brackets. ^bTested in Middlebrook 7H9 broth supplemented with 0.2% glycerol, 0.05% tween 80, and 10% OADC. ^cTested in cation-adjusted Mueller Hinton II Broth (CAMHB).

μM) moiety. While the potency was improved, the hydrophobicity of **11** (logD_{7.4} = 3.9) and **12** (logD_{7.4} = 3.4) was increased, which had a slight impact on their solubility (148 and 133 μM, respectively). To address this, the phenyl group of **11** was replaced by a more polar pyridine group (compound **13**, logD_{7.4} = 2.7), which indeed led to an improved solubility (>200 μM), but at the expense of anti-TB potency (MIC = 0.59 μM) (Table 2). As hypothesized, substitution of the phenyl ring prevented metabolism on this part of the molecule (Figure S2). However, microsomal stability remained only partially improved compared to compound **1**. Overall, study of

these first SARs for compound **1** allowed for marked improvements to the TriSLa anti-TB potency.

In Vitro Profiling of TriSLa Activity. Spectrum of TriSLa Antibiotic Activity. The spectrum of TriSLa antibiotic activity was next determined on a panel of mycobacteria as well as Gram-positive and -negative bacteria. Compounds **1**, **11**, and **12** showed mycobacterium-specific activity with *Mtb*, *M. marinum*, and *M. avium* being particularly susceptible (Table 3). Gram-positive and -negative bacteria were found to be resistant to TriSLa activity, including the efflux-deficient *E. coli* ΔtolC (Table 3). These three TriSLa compounds showed no

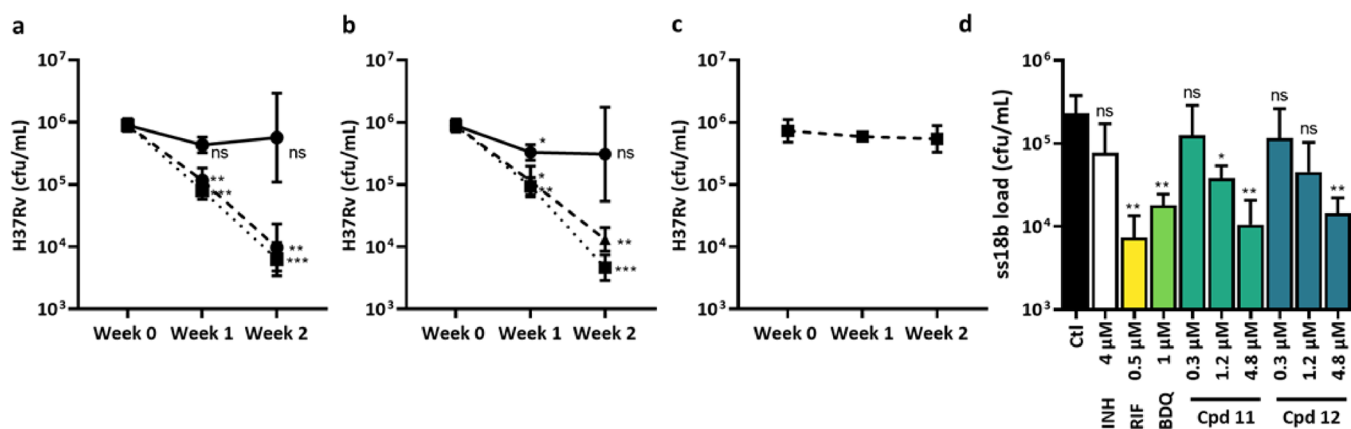


Figure 1. In vitro profile of TriSLAs against replicating H37Rv (a–c) and nonreplicating ss18b (d). The bactericidal activity of (a) **11**, (b) **12**, and (c) bedaquiline was measured by cfu counting following 1 or 2 weeks of incubation with 1× MIC (filled circles, solid line), 2× MIC (filled triangles, dashed line), or 4× MIC (filled squares, dotted line). Data are mean and SEM of at least three independent biological replicates, and statistical analysis was performed with a paired *t*-test. (d) Bactericidal activity following 1-week incubation with TriSLAs and control antibiotics (isoniazid (INH) bedaquiline (BDQ), rifampicin (RIF)) against nonreplicating ss18b-lux as measured by cfu counting. Data are mean and SEM of at least three independent biological replicates, and the statistical test to compare compound exposure to no compound control was performed using a two-tailed unpaired *t* test with Welch's correction. The time-dependent decrease in ss18b-lux luminescence is available in Figure S3.

apparent cytotoxicity on BALB/3T3 cells at concentrations up to 100 μM.

Time-Dependent Bactericidal Activity of TriSLAs on Replicating and Nonreplicating *M. tuberculosis*. To evaluate the bactericidal activity of TriSLAs in vitro, the bacterial load (measured by colony forming units, cfu) was determined after 1 and 2 weeks of compound exposure at 1×, 2×, and 4× MIC. Data revealed that 1× MIC values of both **11** and **12** (150 nM) were bacteriostatic, while exposure to 2× and 4× MIC (300 and 600 nM) led to around a 0.8-log and 2.0 log drop in cfu after 1 and 2 weeks, respectively (Figure 1a,b). In line with previous reports,²⁴ bedaquiline at 1× and 2× MIC (250 and 500 nM, respectively) was largely bacteriostatic over the 2 week exposure period (Figure 1c).

The activity of TriSLA compounds was then evaluated on nonreplicating bacteria using a luciferase-expressing streptomycin starved 18b model of nonreplicating *Mtb* (ss18b-lux²⁵). By monitoring the ss18b-lux luminescence signal from the integrated *luxCDABE* reporter, a time-dependent decrease in luminescence was observed with rifampicin, bedaquiline, and the TriSLAs **11** and **12**, while isoniazid caused an increase in luminescence, as reported previously for cell wall inhibitors (Figure S3). This bactericidal activity was confirmed by plating of the remaining ss18b-lux bacteria following 7 days of antibiotic exposure on streptomycin-containing plates and cfu counting. Data clearly show that exposure to high concentrations of isoniazid had no significant bactericidal activity against nonreplicating ss18b-lux, while rifampicin and bedaquiline were bactericidal, as previously reported.^{25,26} In this assay, both **11** and **12** showed a concentration-dependent killing of ss18b-lux, with concentrations of 4.8 μM leading to a 1–2 log drop in bacterial counts, similar to that seen for 1 μM bedaquiline and 0.6 μM rifampicin (Figure 1d), while the potency of **11** and **12** are lower than that observed on replicating bacteria.

TriSLA Activity on Intracellular *M. tuberculosis*. To define the activity of the TriSLA compounds against intracellular *Mtb*, their ability to protect differentiated THP-1 macrophages from a lethal infection dose of H37Rv was evaluated as a proxy to the number of intracellular bacteria. Data showed that control

compounds isoniazid (IC₅₀ = 204 ± 20 nM), rifampicin (IC₅₀ = 91 ± 32 nM), and bedaquiline (IC₅₀ = 34 ± 3 nM) were able to fully protect the macrophages from infection, in line with previously described data (Figure S4). The TriSLA compounds tested were found to also protect macrophages from death by the intracellular infection in a similar hierarchy to that observed on extracellular H37Rv (Table 2), but protection was not absolute (did not achieve 100% protection) and required higher concentrations (Figure S4), suggesting that TriSLAs are less effective on intracellular bacteria than isoniazid, rifampicin, or bedaquiline.

Target Identification of TriSLAs. To gain insight into the mechanism of action of the TriSLA series, resistant *Mtb* mutants were isolated and characterized. After exposure to compound **1** at 14 and 28 μM, resistant H37Rv isolates were selected at a frequency of around 1 × 10⁻⁸ (six and four colonies, respectively, following the plating of 50 μL of OD₆₀₀ = 50), with confirmation of resistance to **1** by REMA (MIC > 100 μM). Whole genome sequencing and variant analysis of two resistant isolates found one (RC14.2) to carry a 97 bp base-pair deletion in the *ndhA* (Rv0392c) promoter (including a 17 bp truncation of the 5' end of neighboring, nonessential Rv0393 (encoding a 13E12 repeat family protein)) (Figure S5), and the other (RC28.2) to carry a nonsynonymous single nucleotide polymorphism in *ndh* (Rv1854c) leading to Tyr403Cys (Table S2) (sequences available at NCBI project number, PRJNA808942). Similarly, validated **11**-resistant clones of H37Rv were isolated on 1 μM **11** at a frequency of resistance at around 3 × 10⁻⁷, and Sanger sequencing of *ndh* and *ndhA* (including promoter) found them to carry an alternative nonsynonymous mutation in the same *ndh* codon leading to Tyr403His and Tyr403Asn (Table S2). Finally, *M. marinum* isolates resistant to **11** were selected through sequential selection in liquid culture containing 4 μM TriSLA, followed by isolation of single clones on solid culture (direct selection on solid media led to high background). Sanger sequencing revealed these clones to similarly carry nonsynonymous mutations in *ndh* (MMAR_2728), but this time in conserved Gln334 codon, leading to Gln334Pro or Gln334Arg substitutions (Table S2).

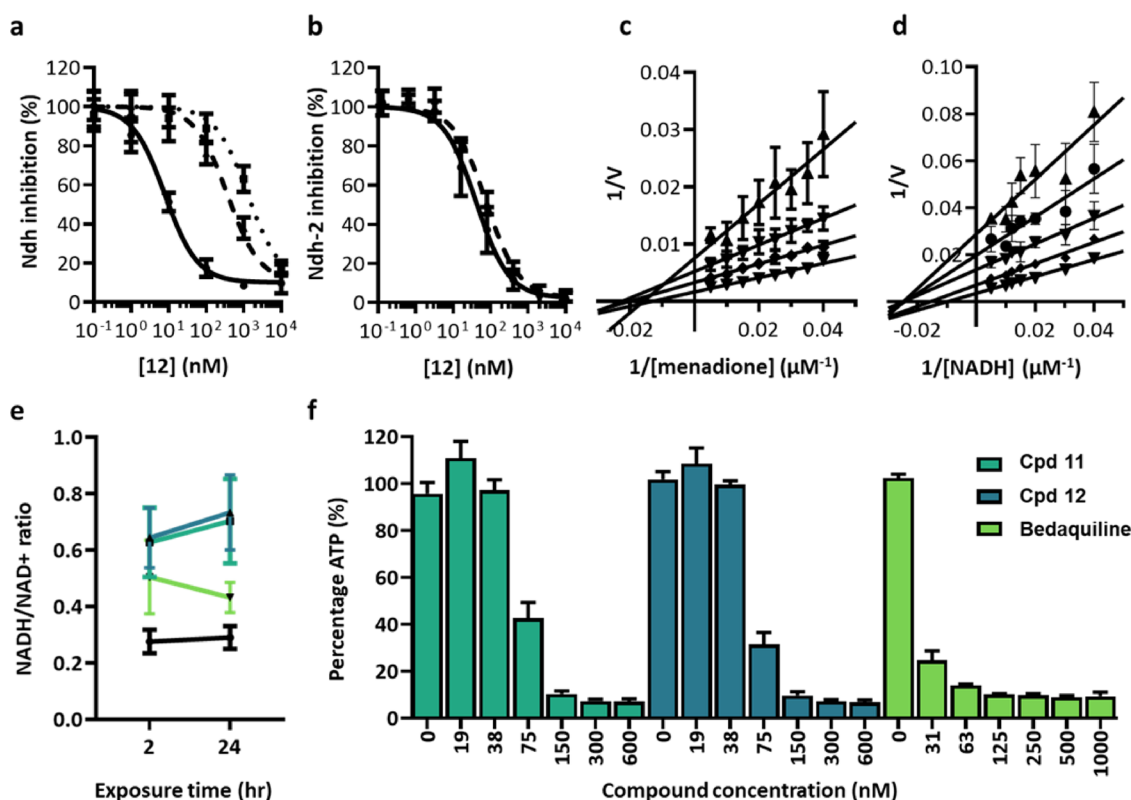


Figure 2. Biochemical target validation of TriSLAs and impact on the *Mtb* electron transport chain. (a) Compound 12 biochemical inhibition of NADH oxidation by recombinant *Mtb* MBP-Ndh (filled circles, solid line), MBP-Ndh(Y403C) (filled triangles, dashed line), and MBP-Ndh(Q334P) (filled squares, dotted line) overexpressed and purified using *E. coli*. Data are presented as a mean \pm SD of at least three independent biological replicates. (b) Compound 12 biochemical inhibition of NADH oxidation by recombinant *Mtb* MBP-Ndh (filled circles, solid line) and MBP-NdhA (filled triangles, dashed line) overexpressed and purified using *M. smegmatis*. (c) Lineweaver–Burk plot showing noncompetitive inhibition of Ndh by 12 relative to menadione ($n \geq 3$), (d) Lineweaver–Burk plot showing noncompetitive inhibition of Ndh by 12 relative to NADH ($n \geq 3$), (e) *Mtb* NADH/NAD⁺ ratios measured following 2 and 24 h exposure to 11 (green-blue, 600 nM, 4 \times MIC), 12 (dark blue, 600 nM, 4 \times MIC), and bedaquiline (green, 1 μ M, 4 \times MIC), compared to unexposed DMSO controls (black) ($n \geq 3$), and (f) *Mtb* ATP concentrations measured following 24 h exposure to either 11 (green-blue), 12 (dark blue), and bedaquiline (green) ($n \geq 3$).

Both *ndh* and *ndhA* encode for the two *Mtb* type II NADH dehydrogenases (Ndh-2: Ndh, and NdhA) of the bacterial electron transport chain that mediate the transfer of electrons from NADH to menaquinone. Ndh and NdhA share 67% protein identity, with both Tyr403/Gln334 and surrounding amino acids conserved (Figure S6). In the absence of a protein structure of Ndh (or NdhA), structural models were generated by AlphaFold^{27,28} and by homology (using SwissModel). Tyr403 and Gln334 were found in close proximity to each other (with a hydrogen bond interaction between their side chains according to AlphaFold) near the access pocket of menaquinone in the membrane-associated region of the protein (Figure S7). To date, mutations in this region of Ndh have not been associated with resistance to any antibiotic molecule. On the other hand, a deletion in the *ndhA* promoter (different to the one isolated here) that leads to an overexpression of *ndhA* has previously been isolated following selection to the 2-mercapto-quinazolinone family of Ndh-2 inhibitors.²⁹ In line with this, RT-qPCR found that the 97-base pair deletion found in the *ndhA* promoter of RC 14.2 had a 23-fold increased expression of *ndhA* relative to the parental strain, while expression of *ndh* remained unchanged (Table S3).

Biochemical Inhibition of Ndh-2 by TriSLAs. To confirm that TriSLAs are Ndh-2 inhibitors, initial validation experiments focused Ndh, the primary NADH dehydrogenase in *Mtb*.³⁰ Using published methodology,²⁹ recombinant

maltose-binding protein (MBP)-tagged Ndh (MBP-Ndh) was produced and purified from *E. coli* Rosetta cells and confirmed to be active and reduce the surrogate electron acceptor menadione in the presence of NADH. Inhibition studies found that TriSLAs were a nanomolar inhibitor of NADH oxidation by MBP-Ndh (Table 1) and that this biochemical inhibition was in direct correlation with TriSLa MIC on *Mtb* (Figure S8). Biochemical evaluation of MBP-Ndh (Tyr403Cys) and MBP-Ndh (Gln334Pro) found these mutant proteins to be active, but 30–60 fold and 70–200 fold more resistant than MBP-Ndh to TriSLa-mediated inhibition, respectively (Figure 2a, Table S4). To determine if TriSLAs also inhibit NdhA, a codon-optimized MBP-NdhA was overexpressed and purified from *M. smegmatis* (recombinant MBP-NdhA purified from *E. coli* Rosetta was found to have poor catalytic activity), and inhibition studies found TriSLAs to inhibit MBP-NdhA in a similar manner to MBP-Ndh (Figure 2b). Together, these data validate TriSLAs as pan-Ndh-2 inhibitors and confirm the importance of Tyr403 and Gln334 for TriSLa-mediated inhibition of Ndh.

TriSLAs Are Noncompetitive Inhibitors of Ndh. As mentioned above, TriSLa resistance conferring mutations in Ndh (Tyr403 and Gln334) are located near the menaquinone-binding pocket of Ndh, suggesting that TriSLAs could act as competitive inhibitors for menaquinone binding. Biochemical competition assays with varying concentrations of menadione

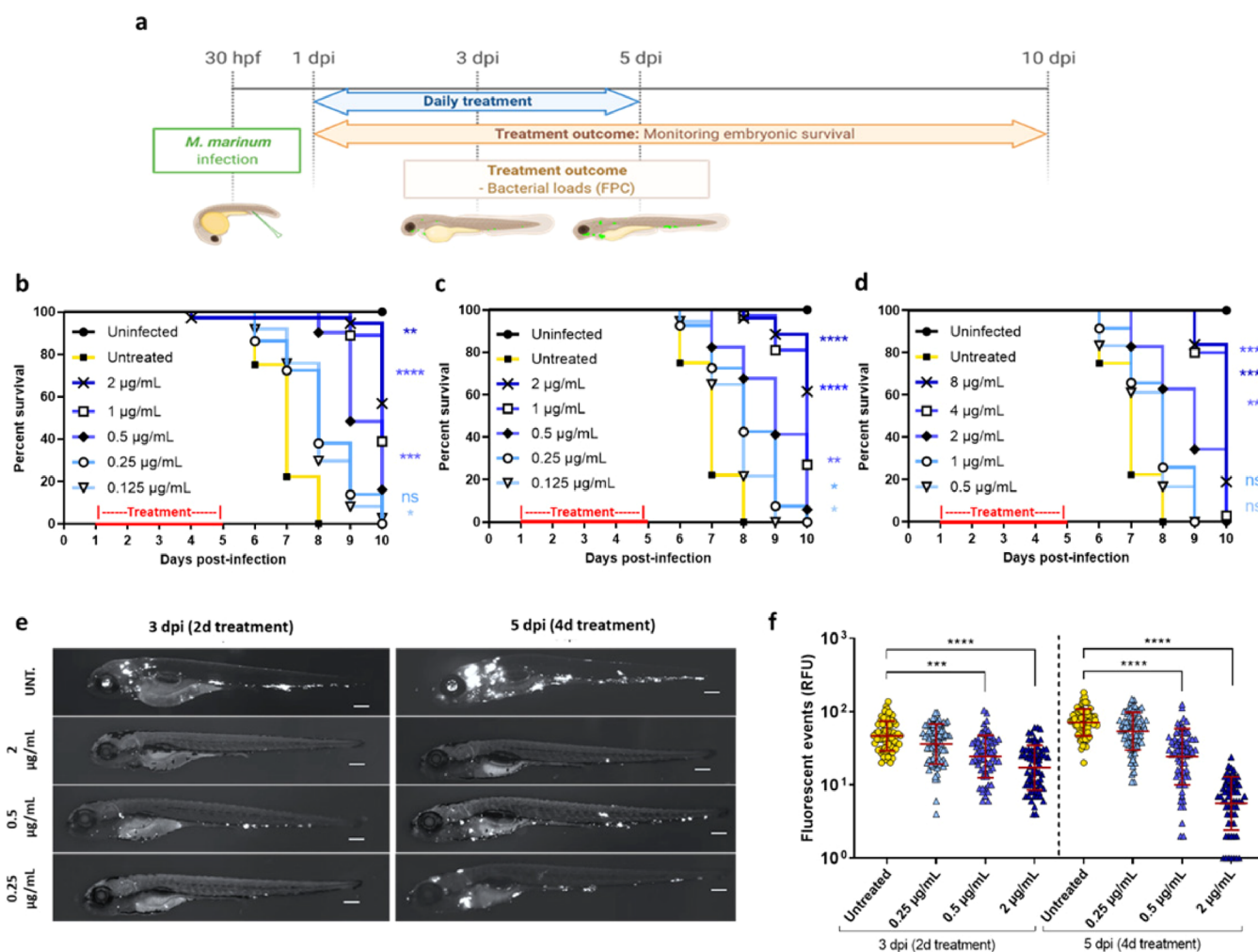


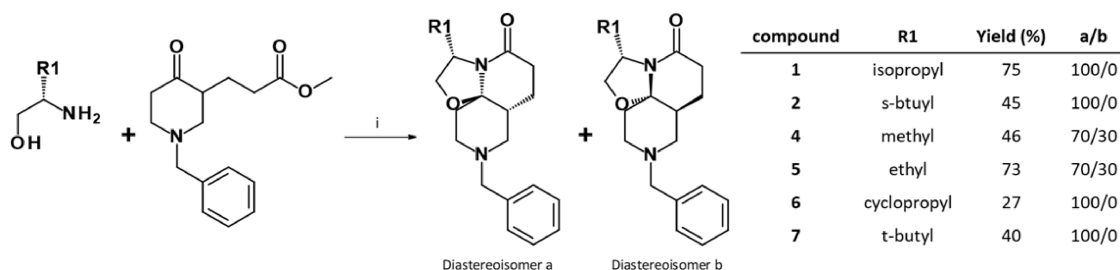
Figure 3. In vivo efficacy of TriSLAs against *M. marinum*-infected embryonic zebrafish. (a) Schematic of the in vivo efficacy protocol showing the timeline of zebrafish embryo infection (200–250 colony-forming units (cfu) *M. marinum* expressing Wasabi), the exposure period to different concentrations of TriSLAs (daily changes), and compound washout. hpf: hours post-fertilization; dpi: days post-infection; FPC: Fluorescence pixel count. (b–d) Survival curve of *M. marinum*-infected zebrafish embryos monitored over the 10-day period post-infection, with and without 4-day treatment of (b) compound 11, (c) compound 12, and (d) compound 13. Survival curves are the cumulative results of three experiments covering more than 25 infected zebrafish per group. Statistics to compare treatment groups were performed using the log rank (Mantel–Cox) statistical test ($*P < 0.05$, $**P < 0.01$, $****P < 0.0001$). (e) Representative sequential fluorescence images of *M. marinum* (Wasabi) infected zebrafish embryos following 2 or 4 days of treatment (3 and 5 dpi) with compound 12 at 0.25, 0.5, and 2 $\mu\text{g/mL}$, relative to untreated zebrafish (UNT). Scale bar, 210 μm . (f) *M. marinum* infection burden in zebrafish embryo as quantified following 2 (3 dpi) and 4 (5 dpi) days of compound 12 exposure (0.25, 0.5, and 2 $\mu\text{g/mL}$) by pixel count (fluorescent events) using the ImageJ software. The data presented are the cumulative data of three independent experiment (each containing 20 to 25 embryos per group), with each data point representing one infected zebrafish larva. The error bar represents the mean and standard deviations of the cumulative dataset. Statistical comparison of the different groups was performed using a Mann–Whitney’s *t* test, ($***P < 0.001$, $****P < 0.0001$).

(model electron acceptor) or NADH however suggest TriSLAs to not compete with either cofactor and instead inhibit Ndh through a noncompetitive or allosteric mechanism (Figure 2c,d).

Impact of TriSLAs on the Bacterial Electron Transport Chain. As inhibitors of Ndh-2, TriSLAs were expected to impact the bacterial NADH/NAD⁺ ratio and the functioning of the electron transport chain. To confirm this, NADH and NAD⁺ concentrations were measured in *Mtb* following 2 and 24 h of exposure to 4× MICs of 11 or 12 (600 nM). Relative to untreated bacteria, TriSLA-exposed bacteria showed an increase in the NADH/NAD⁺ ratio, driven by an increase in NADH and decrease in NAD⁺ (Figure 2e). As previously published,²⁴ exposure to bedaquiline also caused an increase in the NADH/NAD⁺ ratio as a result from “back-pressure” on the

electron transport chain, while rifampicin induced a decrease in NADH/NAD⁺. TriSLAs were also found to impact the electron transport chain as a whole, as exposure to 12 and 11 (Figure 2f) caused a concentration-dependent shutdown in bacterial ATP concentrations, similar to that observed following exposure to bedaquiline (Figure 2f). Together, these data support that inhibition of Ndh-2 in *Mtb* has a major impact on the bacterial electron transport chain leading to a decrease in ATP production.

Impact of Media Composition on TriSLA Antibiotic Activity. Recent work has shown Ndh-2 to not be essential for *Mtb* growth in the absence of fatty acids and that the removal of all fatty acids from the culture medium rendered Ndh-2 inhibitors such as 2-mercapto-quinazolinones inactive.³¹ To verify this impact, the activity of TriSLAs was re-evaluated in

Scheme 1. Synthesis of Analogues 1–7^a

^aReagents and conditions: (i) methyl 3-(1-benzyl-4-oxo-3-piperidyl)propanoate (1 equiv), amino-alcohol (1.2–3 equiv), pivalic acid (1.2–3 equiv), toluene, 150 °C (thermic for 20 h or microwave irradiations for 1–4 h).

media lacking fatty acids (using fatty acid-free BSA), and data confirmed that the MIC of the compounds **1**, **11**, and **12** and a control 2-mercapto-quinazolinones/thioquinazoline (CBR-5992) all increased significantly, while no impact was observed for rifampicin or bedaquiline (Table S5). To confirm that this impact is not *Mtb* specific, the role of fatty acids in the culture medium was also evaluated on *M. marinum*, confirming the same dependence of fatty acids for TriSLa activity (Table S5). Other published work showed that mutations in *ndh* of *M. smegmatis* and *M. bovis* BCG rendered these bacteria auxotrophic for serine³² and that L-serine supplementation to the media rendered the Ndh-2 inhibitors (CBR-1825) less potent against *Mtb* in vitro.³³ In accordance with these results, supplementation of L-serine to the growth medium also caused a loss of antibiotic activity of the TriSLa compounds against H37Rv (Table S6). Finally, the detergents (Tween 80 or tyloxapol or neither) used in the culture media were not found to have impact on TriSLa activity (Table S6).

In Vivo Efficacy on *M. marinum*-Infected Zebrafish.

Considering the influence of media components on TriSLa antibiotic activity, it was considered a priority to evaluate the in vivo efficacy of TriSLa compounds. As the in vitro metabolic stability of the TriSLa compounds (Table S1) was too low for progression into murine efficacy studies of *Mtb* infection, it was decided to evaluate the in vivo efficacy of TriSLas on *M. marinum* infected zebrafish larvae, where compound exposure in the water is more stable. In such studies on acutely *M. marinum*-infected zebrafish larvae, the mycobacteria are phagocytosed by circulating macrophages and aggregate into foci that start to resemble granuloma.^{34–37} Initial toxicity experiments confirmed that compounds **11**, **12**, and **13** did not interfere with larval development or show any toxicity in noninfected zebrafish larvae (data not shown). Next, efficacy studies were performed as previously,³⁴ where zebrafish larvae infected with *M. marinum* (expressing Wasabi) were exposed to different doses of TriSLas (refreshed daily) for a 4-day period (from 1 to 5 days post-infection (dpi)), followed by a 5-day period in the absence of antibiotics where survival was monitored (Figure 3a). Data confirmed that 4-day exposure compounds **11**, **12**, and **13** significantly prolonged the survival of the infected zebrafish in a dose-dependent manner, starting from doses of 0.3, 0.3, and 1.2 μM (respectively), with higher doses of 4.8, 4.8, and 9.6 μM (respectively) prolonging survival by 3 days (Figure 3b–d). In complement, the bacterial load of the infected zebrafish was determined by fluorescence microscopy during the treatment phase of the study (at 2 and 4 days of exposure).

Images of untreated infected larvae showed an intense dissemination of the *M. marinum* infection, with multiple large

bacterial foci that increased over time (3 and 5 dpi) (Figure 3e), while 2 or 4-day treatment with 0.25 to 2 $\mu\text{g}/\text{mL}$ (0.6–4.8 μM) of **12** clearly resulting in fewer and less intense infection foci (Figure 3e). Quantification of the bacterial load on a larger number of infected zebrafish (using fluorescence pixel count determination) showed that exposure to 0.5 $\mu\text{g}/\text{mL}$ (1.2 μM) of **12** was bacteriostatic, preventing an increase in bacterial load from 2–4 days of exposure, while higher doses of 2 $\mu\text{g}/\text{mL}$ (4.8 μM) lead to a significant decrease in the bacterial burden between 2 and 4 days of over the same period (Figure 3f). Together, these data confirm that inhibition of Ndh-2 has a significant impact on *M. marinum* infection in the zebrafish model of infection.

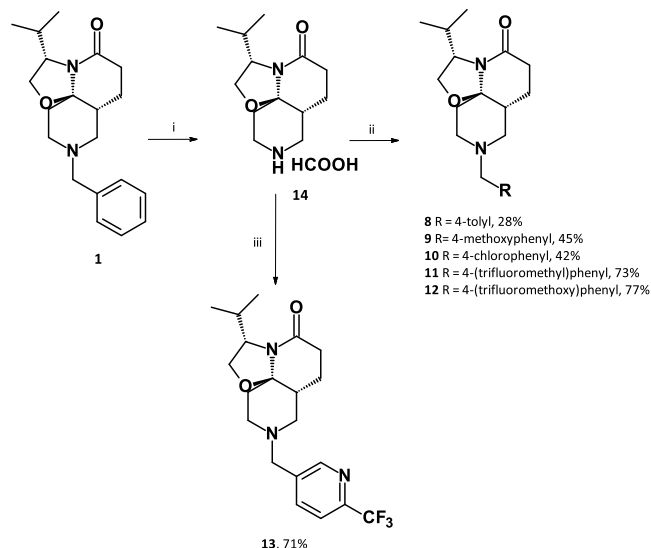
Chemistry. The unique rigid 3D TriSLa core of the previously described molecules was obtained through stereoselective Meyers' lactamization.^{17,38} This reaction uses readily accessible starting materials such as keto-esters (or keto-acids) as bi-electrophile and amino alcohols as bi-nucleophiles to generate complex-fused ring systems. Lactams **1**–**7** were obtained by reacting methyl 3-(1-benzyl-4-oxo-3-piperidyl)propanoate (obtained by esterification of its acid analogue, previously synthesized according to the literature)¹⁷ with the appropriate β -amino alcohol (Scheme 1) in yields ranging from 27 to 75%. Only partial stereoselectivity was observed with mildly hindered β -amino alcohols (compounds **4** and **5**), while only one stereoisomer was obtained with highly hindered β -amino alcohols (compounds **1**, **2**, **6**, and **7**).

Analogues **8**–**13** were synthesized from compound **1** (Scheme 2), through *N*-debenzylation using Pd/C and ammonium formate followed by *N*-alkylation using nucleophilic substitutions (compounds **8**–**12**) or reductive amination (compound **13**).

DISCUSSION

Natural products and their hemisynthetic derivatives are a rich source of bioactive molecules and make up the bulk of the antibiotic classes currently used. Natural products often boast an increased chemical complexity,^{39,40} particularly emphasized by an abundance of chiral tetrahedral carbons. This increased 3D aspect allows natural products to occupy a different biological space compared to flatter molecules found in many drug-like screening collections. In this work, we demonstrate that screening synthetic focused chemical libraries enriched with nature-inspired scaffolds is a promising approach to identify novel antituberculosis chemical scaffolds with potent activity.

In recent years, a number of anti-TB molecules targeting Ndh-2 have been described, including 2-mercapto-quinazolinones,^{29,33} quinolones,^{41,42} and quinolinyl-pyrimidines,^{43,44}

Scheme 2. Synthesis of Analogues 8–13^a

^aReagents and conditions: (i) Pd/C 10% (10 mol %), HCO₂H (5 equiv), reflux, 30 min; (ii) 14 (1 equiv), K₂CO₃ (3 equiv), RCH₂Br (1–1.5 equiv), NaI (0–1 equiv), MeCN, RT, 1–20 h; (iii) 14 (1 equiv), 6-(trifluoromethyl)pyridine-3-carbaldehyde (3.6 equiv), Ti(OiPr)₄ (1.8 equiv), NaBH(OAc)₃ (3.6 equiv), dichloroethane, RT, overnight.

though no in vivo efficacy studies have been conducted thus far for these inhibitors. Overall, these inhibitors share similar structural features, being largely planar (large number of sp²-hybridized atoms) and carrying a central bicyclic aromatic ring, in sharp contrast to the highly 3D (large number of sp³-hybridized atoms) structure of the TriSLa compounds described here. Despite these structural differences, TriSLAs do share common attributes with the most potent of these compounds, (2-mercapto-quinazolinones^{29,33}). This includes comparable potency, being pan Ndh-2 inhibitors, being noncompetitive inhibitors of Ndh, displaying activity modulated by promoter mutation in *ndhA*, by L-serine and by fatty acid content in the media. Having structurally diverse chemical scaffolds targeting a protein is particularly worthwhile in drug development as this allows for different ADME/Tox profile and provides an alternative in case of drug development flags such as toxicity, pharmacokinetics (including tissue distribution), and off-target effects that are more often associated with the chemical scaffold. Together, this will help increase the chance of Ndh-2 inhibitors to enter clinical development. In this study, we report point mutations in Ndh that confer resistance to TriSLAs, suggesting that these inhibitors act specifically at the Ndh-2 protein-membrane interface. Multiple protein alignment of Ndh-2 orthologues from a panel of bacteria shows Gln344 to be highly conserved between bacteria, while Tyr403 is conserved amongst mycobacteria, which likely explains their mycobacteria-specific antibacterial spectrum. Ndh structure models computed using AlphaFold^{27,28} interestingly place the side chains of Tyr403 and Gln344 in close proximity to each other with possible hydrogen bonding interactions between their side chains. These residues are likely flexible, but in the model these interacting residues appear to greatly limit the size of the menaquinone access pocket (Figure S8). A hypothesis on the mechanism of Ndh-2 inhibition by TriSLAs is that they bind

and stabilize this closed conformation and hence prevent the access of menaquinone, thus preventing its subsequent reduction. However, future structural biology efforts are needed to further elucidate how these two potent inhibitors are acting on Ndh-2.

Recent work demonstrated that *Mtb* could survive in vitro without either of its *ndh-2* genes when grown in the absence of exogenous fatty acids³¹ and that this double *ndh-2* deleted strain could still infect mice, though it was partially attenuated with a 26-fold lower maximal titre.³¹ As demonstrated for 2-mercapto-quinazolinones Ndh-2 inhibitors,³¹ the removal of all fatty acids from the media, or additional serine supplementation (greater than natural available concentration) also prevent the activity of TriSLAs in vitro, confirming the vulnerability of Ndh-2 in the presence of fatty acids. Together, this work called into question the potential of Ndh-2 inhibitors in the fight against tuberculosis infections, and reasons that efficacy will depend on the fatty acid content of the compartments in which the mycobacteria reside. Data presented here highlight that despite TriSLa activity on *M. marinum* also being dependent on fatty acids, TriSLa treatment of *M. marinum*-infected zebrafish did result in concentration-dependent efficacy, both prolonging zebrafish survival and decreasing bacterial loads. This therefore evokes that, at least in this infection model, a significant proportion of *M. marinum* is likely to reside in a fatty acid-containing compartment, such as granuloma type structures, which are considered fatty acid-rich. Indeed, recent work has shown that the zebrafish/*M. marinum* granuloma contains the lipid-rich foam cells and that this differentiation of macrophages into foam cells is stimulated by the mycobacterial ESX-1 type VII secretion locus.⁴⁵

This observed efficacy is, however, in contrast to the aforementioned finding that despite partial attenuation, Ndh-2 double knockout *Mtb* strains could still grow in C57BL/6 mice.³¹ Apart from possible differences in Ndh-2 vulnerability in *Mtb* and *M. marinum*, differences in the bacterial compartmental distribution (such as granulomas, intracellular, extracellular) and its associated fatty acid content may also be a factor to consider. In *Mtb*-infected C57BL/6 mice, the infection is largely believed to reside within macrophages, where the primary carbon source is expected to be cholesterol (depending on the macrophage) and where fatty acid availability is likely lower than in granulomas. TriSLAs (and 2-mercaptoquinoxalines) are poorly active against these intracellular infections and may hence contribute to this difference. As granuloma are believed to play a major role in human *Mtb* infections, more work is needed to define the exact vulnerability of Ndh-2, and the potential of Ndh-2 inhibitors as anti-TB agents alone and in combination in animal models where granuloma formation is observed. For that purpose, further efforts will all focus on generating TriSLa compounds with an optimal pharmacokinetic profile.

Together, this work presents a new antimycobacterial chemical scaffold that acts through allosteric inhibition of Ndh-2. In vitro profiling of the TriSLAs showed them to have a time-dependent bactericidal activity on replicating and non-replicating bacteria, and in vivo efficacy studies confirm the vulnerability of this protein in *M. marinum* infected zebrafish. Future medicinal chemistry will aim to confirm Ndh-2 vulnerability for *Mtb* in various murine models of infection, and define TriSLa based treatment regimens.

EXPERIMENTAL SECTION

Chemical Synthesis. General Information. All reagent-grade chemicals and anhydrous solvents for synthesis, analysis, and purification were obtained from commercial suppliers and were used as received without further purification.

Flash chromatography was performed using a Puriflash PF-430 with silica gel cartridges (Buchi silica 40 μm). ELSD and UV detection (254 nm) were used to collect the desired product. Reverse flash chromatography was performed using a CombiFlash Rf200 with C18 cartridges (Buchi C18 40 μm). UV detection (215 and 254 nm) was used to collect the desired product.

^1H NMR and ^{13}C NMR spectra were recorded on a Bruker DRX-300 spectrometer. Chemical shifts (δ) are in parts per million (ppm). The ^1H spectra were calibrated to signals from CD_2Cl_2 (δ 5.36 ppm) or CDCl_3 (δ 7.26 ppm), and ^{13}C spectra from CD_2Cl_2 (δ 53.5 ppm) or CDCl_3 (δ 77.16 ppm). ^1H NMR spectra are reported as follows: chemical shift (ppm), multiplicity (s: singlet; brs: broad singlet; d: doublet; dd: doublet of doublet; t: triplet; td: triplet of doublet; m: multiplet), coupling constants in Hertz (Hz) and integration. Proton and carbon signal assignments were established using COSY, HSQC-DEPT, and HMBC spectra.

Liquid chromatography–mass spectrometry (LC–MS) Waters system was equipped with a 2747 sample manager, a 2695 separation module, a 2996 photodiode array detector (200–400 nm), and a Micromass ZQ2000 detector (scan 100–800). An XBridge C18 column (50 mm \times 4.6 mm, 3.5 μm , Waters) was used. The injection volume was 20 μL . A mixture of water and acetonitrile was used as the mobile phase in gradient-elution. The pH of the mobile phase was adjusted with HCOOH and NH_4OH to form a buffer solution at pH 3.8. The analysis time was 5 min (at a flow rate of 2 mL/min), 10 min (at a flow rate of 1 mL/min), or 30 min (at a flow rate of 1 mL/min). Purity (%) was determined by reversed-phase high-performance liquid chromatography (HPLC), using UV detection (215 nm). All final compounds showed purity greater than 95%.

High-resolution mass spectra (HRMS) analysis was performed on a LC–MS system equipped with a LCT Premier XE mass spectrometer (Waters), using a XBridge C18 column (50 mm \times 4.6 mm, 3.5 μm , Waters). A gradient starting from 98% H_2O 5 mM ammonium formate pH 3.8 and reaching 100% MeCN 5 mM ammonium formate pH 3.8 within 3 min at a flow rate of 1 mL was used.

Methyl-3-(1-benzyl-4-oxo-3-piperidyl)propanoate. To a solution of 3-(1-benzyl-4-oxo-3-piperidyl)propanoic acid (19.3 g, 73.9 mmol) in methanol (200 mL) was added SOCl_2 (5.9 mL, 81.3 mmol) dropwise at room temperature. The mixture was then stirred at 55 $^\circ\text{C}$ for 1 h. The solvent was removed under vacuum, and the mixture was dissolved in 0.1 N HCl (100 mL) and stirred at room temperature for 1 h. A saturated aqueous solution of Na_2CO_3 was added until pH 10. The solution was extracted with ethyl acetate. The organic layer was dried over MgSO_4 , and the solvent was removed under reduced pressure to give the crude product, which was purified by silica gel chromatography (cyclohexane/ethyl acetate: 70/30 to 0/100) to afford methyl 3-(1-benzyl-4-oxo-3-piperidyl)propanoate (6.73 g, 33%), as a colorless oil. ^1H NMR (300 MHz, CD_2Cl_2): δ 7.36–7.25 (m, 5H), 3.64 (d, J = 13.1 Hz, 1H), 3.61 (s, 3H), 3.57 (d, J = 13.1 Hz, 1H), 3.08–2.97 (m, 2H), 2.62–2.11 (m, 7H), 2.08–1.95 (m, 1H), 1.53–1.42 (m, 1H) ppm. [ES+ MS] m/z 276 (MH+). ^1H NMR data matched those reported previously (Idzik, T. J.; Myk, Z. M.; Peruzynska, M.; Maciejewska, G.; Drozdziak, M.; Sosnicki, J. G. Arylation of enolactams using TIPSOTf: reaction scope and mechanistic insight. *Org. Chem. Front.* 2021, 8, 708–720).

General Protocol 1: Diastereoselective Meyers' Lactamization. A solution of pivalic acid (1.2–3 equiv) in toluene (0.2 N) was added to methyl 3-(1-benzyl-4-oxo-3-piperidyl)propanoate (1 equiv). The appropriate amino-alcohol (1.2–3 equiv) was added (when the amine is used as a chlorohydrate, DIEA (1.2–3 equiv) was added). The mixture was refluxed at 150 $^\circ\text{C}$ (thermic for 20 h or microwave irradiations for 1–4 h). When the conversion of the keto-ester was judged completely by LC/MS, the solution was dissolved in H_2O and extracted with ethyl acetate or dichloromethane. The layers were

separated. The organic layer was dried over MgSO_4 , filtered, and concentrated under vacuum to give the crude product, which was purified, to afford the corresponding desired product.

(3S,7aR,11aR)-9-Benzyl-3-isopropyl-2,3,6,7,7a,8,10,11-octahydrooxazolo[2,3-j][1,6]naphthyridin-5-one (1). The product 1 was obtained from L-valinol using general protocol 1. The crude product was purified by flash chromatography column over silica (cyclohexane/ethyl acetate: 1/0 to 6/4) to afford the desired product 1 (yield = 75%, white powder) as a single diastereoisomer. ^1H NMR (300 MHz, CDCl_3): δ 7.33–7.20 (m, 5H, $^{\text{Ar}}\text{CH}$), 4.13–4.03 (m, 1H, ^3CH), 3.98 (dd, J = 8.6, 7.6 Hz, 1H, $^2\text{CH}_2$), 3.77 (dd, J = 8.6, 6.2 Hz, 1H, $^2\text{CH}_2$), 3.54 (d of AB system, J = 13.3 Hz, 1H, $^{12}\text{CH}_2$), 3.41 (d of AB system, J = 13.1 Hz, 1H, $^{12}\text{CH}_2$), 2.77–2.64 (m, 2H, $^{10}\text{CH}_2$ and $^8\text{CH}_2$), 2.62–2.51 (m, 1H, $^6\text{CH}_2$), 2.49–2.29 (m, 3H, $^8\text{CH}_2$, $^7\text{CH}_2$ and $^6\text{CH}_2$), 2.25–2.16 (m, 1H, $^{10}\text{CH}_2$), 2.09–1.89 (m, 2H, ^{13}CH and $^{11}\text{CH}_2$), 1.83–1.73 (m, 1H, $^{11}\text{CH}_2$), 1.72–1.55 (m, 2H, ^7CH , and $^7\text{CH}_2$), 0.94 (d, J = 6.8 Hz, 3H, 14 or $^{15}\text{CH}_3$), 0.90 (d, J = 6.8 Hz, 3H, 14 or $^{15}\text{CH}_3$) ppm. ^{13}C NMR (75 MHz, CDCl_3): δ 170.2 (^5CO), 138.9 ($^{\text{Ar}}\text{Cq}$), 128.7, 128.3, 127.0 ($^{\text{Ar}}\text{CH}$), 92.7 ($^{11\text{a}}\text{Cq}$), 66.2 ($^2\text{CH}_2$), 62.5 ($^{12}\text{CH}_2$), 61.2 (^3CH), 54.8 ($^8\text{CH}_2$), 50.7 ($^{10}\text{CH}_2$), 40.4 (^7CH), 32.4 (^{13}CH), 32.4 ($^{11}\text{CH}_2$), 30.8 ($^6\text{CH}_2$), 21.9 ($^7\text{CH}_2$), 19.9 (14 or $^{15}\text{CH}_3$), 18.7 (14 or $^{15}\text{CH}_3$) ppm. HRMS (ESI, m/z): [M + H] $^+$ calcd for $\text{C}_{20}\text{H}_{29}\text{N}_2\text{O}_2$, 329.2229; found 329.2227.

(3S,7aR,11aR)-9-Benzyl-3-[(1S)-1-methylpropyl]-2,3,6,7,7a,8,10,11-octahydrooxazolo[2,3-j][1,6]naphthyridin-5-one (2). The product 2 was obtained from (2S,3S)-2-amino-3-methylpentan-1-ol using general protocol 1. The crude product was purified by preparative HPLC using MeCN + 0.1% HCOOH and H_2O + 0.1% HCOOH gradient (9/1 to 0/10) to afford the product 2 (yield = 45%, yellow oil) as a single diastereoisomer. ^1H NMR (500 MHz, CDCl_3): δ 7.39–7.21 (m, 5H, $^{\text{Ar}}\text{CH}$), 4.14 (dd, J = 7.5, 7.3 Hz, 1H, ^3CH), 3.97 (dd, J = 8.8, 7.5 Hz, 1H, $^2\text{CH}_2$), 3.75 (dd, 1H, J = 8.8, 6.9 Hz, 1H, $^2\text{CH}_2$), 3.65–3.38 (m, 2H, $^{12}\text{CH}_2$), 2.76–2.20 (m, 7H, $^{10}\text{CH}_2$, $^8\text{CH}_2$, $^7\text{CH}_2$, and $^6\text{CH}_2$), 1.89–1.54 (m, 5H, ^{13}CH , $^{11}\text{CH}_2$, $^7\text{CH}_2$, and ^7CH), 1.49–1.38 (m, 1H, $^{15}\text{CH}_2$), 1.19–1.05 (m, 1H, $^{15}\text{CH}_2$), 0.89 (t, J = 7.4 Hz, 3H, $^{16}\text{CH}_3$), 0.85 (d, J = 6.8 Hz, 3H, $^{14}\text{CH}_3$) ppm. ^{13}C NMR (125 MHz, CDCl_3): δ 170.3 (^5CO), 138.7 ($^{\text{Ar}}\text{Cq}$), 128.9, 128.5, 127.1 ($^{\text{Ar}}\text{CH}$), 92.2 ($^{11\text{a}}\text{Cq}$), 65.8 ($^2\text{CH}_2$), 62.5 ($^{12}\text{CH}_2$), 60.8 (^3CH), 54.7 ($^{10}\text{CH}_2$), 50.7 ($^8\text{CH}_2$), 40.4 (^7CH), 38.2 (^{13}CH), 32.0 ($^{11}\text{CH}_2$), 30.8 ($^6\text{CH}_2$), 27.2 ($^{15}\text{CH}_2$), 21.9 ($^7\text{CH}_2$), 14.9 ($^{14}\text{CH}_3$), 12.0 ($^{16}\text{CH}_3$) ppm. HRMS (ESI, m/z): [M + H] $^+$ calcd for $\text{C}_{21}\text{H}_{31}\text{N}_2\text{O}_2$, 343.2386; found: 343.2382.

(3R,7aS,11aS)-9-Benzyl-3-isopropyl-2,3,6,7,7a,8,10,11-octahydrooxazolo[2,3-j][1,6]naphthyridin-5-one (3). The product 3 was obtained from (2R)-2-amino-3-methylbutan-1-ol using general protocol 1. The crude product was purified by flash chromatography column over silica (cyclohexane/ethyl acetate: 1/0 to 6/4) to afford the desired product 3 (yield = 61%, colorless oil) as a single diastereoisomer. The data obtained (NMR and HRMS) were the same as the data described for this enantiomer compound 1.

(3S,7aR,11aR)-9-Benzyl-3-methyl-2,3,6,7,7a,8,10,11-octahydrooxazolo[2,3-j][1,6]naphthyridin-5-one (4a) and (3S,7aS,11aS)-9-Benzyl-3-methyl-2,3,6,7,7a,8,10,11-octahydrooxazolo[2,3-j][1,6]naphthyridin-5-one (4b). The products 4a and 4b were obtained from (2S)-2-aminopropan-1-ol using general protocol 1. The crude product was purified by preparative HPLC using MeCN + 0.1% HCOOH and H_2O + 0.1% HCOOH gradient (9/1 to 0/10). A basification and an extraction at 10 pH with a saturated solution of Na_2CO_3 were carried out on the recovered fraction, and the combined organic layers were dried over MgSO_4 . The solvent was removed under reduced pressure the desired to afford products 4a and 4b (yield = 46%, yellow oil), as a mixture of two diastereoisomers (d.r.(4a/4b) = 70/30). Data for the major diastereoisomer 4a: ^1H NMR (300 MHz, CD_2Cl_2): δ 7.38–7.20 (m, 5H, $^{\text{Ar}}\text{CH}$), 4.28–4.06 (m, 2H, ^3CH and $^2\text{CH}_2$), 3.62 (dd, J = 13.0 Hz, J = 1.3 Hz, 1H, $^2\text{CH}_2$), 3.53 (d, J = 13.4 Hz, 1H, $^{12}\text{CH}_2$), 3.42 (d, J = 13.4 Hz, 1H, $^{12}\text{CH}_2$), 2.78–2.63 (m, 2H, $^{10}\text{CH}_2$ and $^8\text{CH}_2$), 2.58–2.15 (m, 5H, $^{10}\text{CH}_2$, $^8\text{CH}_2$, $^7\text{CH}_2$ and $^6\text{CH}_2$), 1.99–1.60 (m, 5H, $^{11}\text{CH}_2$, $^7\text{CH}_2$ and ^7CH), 1.29 (d, J = 6.1 Hz, 3H, $^{13}\text{CH}_3$) ppm. ^{13}C

NMR (75 MHz, CD₂Cl₂): δ 168.9 (⁵CO), 139.4 (^{Ar}Cq), 129.0, 128.5, 127.3 (^{Ar}CH), 92.6 (^{11a}Cq), 69.7 (²CH₂), 62.7 (¹²CH₂), 55.2 (⁸CH₂), 51.7 (³CH), 50.9 (¹⁰CH₂), 40.7 (^{7a}CH), 31.6 (¹¹CH₂), 31.1 (⁶CH₂), 22.9 (⁷CH₂), 20.2 (¹³CH₃) ppm. HRMS (ESI, *m/z*): [M + H]⁺ calcd for C₁₈H₂₅N₂O₂, 301.1916; found: 301.1914.

(3*S*, 7*aR*, 11*aR*)-9-Benzyl-3-ethyl-2,3,6,7,7*a*,8,10,11-octahydrooxazolo[2,3-*j*][1,6]naphthyridin-5-one (**5a**) and (3*S*, 7*aR*, 11*aR*)-9-Benzyl-3-ethyl-2,3,6,7,7*a*,8,10,11-octahydrooxazolo[2,3-*j*][1,6]naphthyridin-5-one (**5b**). The products **5a** and **5b** were obtained from (2*S*)-2-aminobutan-1-ol using general protocol 1. The crude product was purified by preparative HPLC using MeCN + 0.1% HCOOH and H₂O + 0.1% HCOOH gradient (9/1 to 0/10) to afford products **5a** and **5b** (yield = 73%, yellow oil), as a mixture of two diastereoisomers (d.r. (**5a**/**5b**) = 70/30). Data for the major diastereoisomer **5a**: ¹H NMR (300 MHz, CD₂Cl₂): δ 7.42–7.28 (m, 5H, ^{Ar}CH), 4.23–4.04 (m, 2H, ³CH and ²CH₂), 3.76–3.66 (m, 1H, ²CH₂), 3.73 (d, *J* = 13.3 Hz, 1H, ¹²CH₂), 3.59 (d, *J* = 13.3 Hz, 1H, ¹²CH₂), 2.97–2.75 (m, 2H, ¹⁰CH₂ and ⁸CH₂), 2.58–2.15 (m, 5H, ¹⁰CH₂, ⁸CH₂, ⁷CH₂ and ⁶CH₂), 2.09–1.67 (m, 5H, ¹³CH₂, ¹¹CH₂, ⁷CH₂ and ^{7a}CH), 1.50–1.34 (m, 1H, ¹³CH₂), 0.92 (t, *J* = 7.5 Hz, 3H, ¹⁴CH₃) ppm. ¹³C NMR (75 MHz, CD₂Cl₂): δ 169.0 (⁵CO), 136.7 (^{Ar}Cq), 129.3, 128.3, 127.5 (^{Ar}CH), 91.6 (^{11a}Cq), 70.0 (²CH₂), 61.9 (¹²CH₂), 57.0 (³CH), 54.1 (⁸CH₂), 50.0 (¹⁰CH₂), 39.9 (^{7a}CH), 30.6 (¹¹CH₂), 30.6 (⁶CH₂), 27.8 (¹³CH₂), 22.1 (⁷CH₂), 10.2 (¹⁴CH₃) ppm. HRMS (ESI, *m/z*): [M + H]⁺ calcd for C₁₉H₂₇N₂O₂, 351.2017; found: 351.2093.

(3*S*, 7*aR*, 11*aR*)-9-Benzyl-3-cyclopropyl-2,3,6,7,7*a*,8,10,11-octahydrooxazolo[2,3-*j*][1,6]naphthyridin-5-one (**6**). The product **6** was obtained from (2*S*)-2-amino-2-cyclopropyl-ethanol;hydrochloride using general protocol 1. The crude product was purified by preparative HPLC using H₂O + 0.1% HCOOH/MeCN + 0.1% HCOOH (90/10 to 0/100) to afford the desired product **6** (yield = 27%, brown oil), as a single diastereoisomer. ¹H NMR (300 MHz, CDCl₃): δ 7.36–7.23 (m, 5H, ^{Ar}CH), 4.15 (dd, *J* = 8.5 Hz, *J* = 8.4 Hz, 1H, ²CH₂), 3.86 (dd, *J* = 8.9 = 5 Hz, *J* = 6.8 Hz, 1H, ²CH₂), 3.75–3.62 (m, 1H, ³CH), 3.58 (d of AB system, *J* = 13.4 Hz, 1H, ¹²CH₂), 3.44 (d of AB system, *J* = 13.4 Hz, 1H, ¹²CH₂), 2.82–2.18 (m, 6H, ¹⁰CH₂, ⁸CH₂, ⁷CH₂ and ⁶CH₂), 2.11–1.89 (m, 2H, ¹¹CH₂), 1.74–1.54 (m, 2H, ^{7a}CH and ⁷CH₂), 0.93–0.72 (m, 2H, ¹⁴ or ¹⁵CH₂ and ¹³CH), 0.66–0.41 (m, 2H, ¹⁴ or ¹⁵CH₂), 0.30–0.17 (m, 1H, ¹⁴ or ¹⁵CH₂) ppm. ¹³C NMR (75 MHz, CDCl₃): δ 169.4 (⁵CO), 138.9 (^{Ar}Cq), 128.8, 128.4, 127.1 (^{Ar}CH), 92.6 (^{11a}Cq), 68.0 (²CH₂), 62.6 (¹²CH₂), 59.9 (³CH), 54.9 (⁸CH₂), 50.8 (¹⁰CH₂), 40.4 (^{7a}CH), 31.8 (¹¹CH₂), 31.1 (⁶CH₂), 22.5 (⁷CH₂), 15.8 (¹³CH), 4.6 (¹⁴ or ¹⁵CH₂), 2.7 (¹⁴ or ¹⁵CH₂) ppm. HRMS (ESI, *m/z*): [M + H]⁺ calcd for C₂₀H₂₇N₂O₂, 327.2071; found: 327.2073.

(3*S*, 7*aR*, 11*aR*)-9-Benzyl-3-tert-butyl-2,3,6,7,7*a*,8,10,11-octahydrooxazolo[2,3-*j*][1,6]naphthyridin-5-one (**7**). The product **7** was obtained from (2*S*)-2-amino-3,3-dimethyl-butan-1-ol using general protocol 1. The crude product was purified by preparative HPLC using H₂O + 0.1% HCOOH/MeCN + 0.1% HCOOH (90/10 to 0/100) to afford the desired product **7** (yield = 40%, yellow oil), as a single diastereoisomer. ¹H NMR (300 MHz, CD₂Cl₂): δ 7.36–7.19 (m, 5H, ^{Ar}CH), 4.11 (t, *J* = 6.9 Hz, 1H, ³CH), 3.85 (d, *J* = 6.5 Hz, 2H, ²CH₂), 3.53 (d, *J* = 13.3 Hz, 1H, ¹²CH₂), 3.41 (d, *J* = 13.3 Hz, 1H, ¹²CH₂), 2.77–2.69 (m, 1H, ¹⁰CH₂), 2.61–2.57 (m, 1H, ⁸CH₂), 2.58–2.49 (m, 1H, ⁶CH₂), 2.45–2.27 (m, 3H, ⁸CH₂, ⁷CH₂, and ⁶CH₂), 2.20 (dt, *J* = 12.0 Hz, *J* = 3.4 Hz, 1H, ¹⁰CH₂), 1.98 (dt, *J* = 13.3 Hz, *J* = 4.7 Hz, 1H, ¹¹CH₂), 1.90–1.82 (m, 1H, ¹¹CH₂), 1.73–1.52 (m, 2H, ⁷CH₂ and ^{7a}CH), 0.92 (s, 9H, ¹⁴CH₃, ¹⁵CH₃ and ¹⁶CH₃) ppm. ¹³C NMR (75 MHz, CD₂Cl₂): δ 172.7 (⁵CO), 139.5 (^{Ar}Cq), 129.1, 128.5, 127.2 (^{Ar}CH), 94.3 (^{11a}Cq), 64.8 (³CH), 64.5 (²CH₂), 62.7 (¹²CH₂), 54.9 (⁸CH₂), 50.9 (¹⁰CH₂), 40.2 (^{7a}CH), 34.8 (¹³Cq), 32.7 (¹¹CH₂), 31.0 (⁶CH₂), 27.8 (¹⁴CH₃, ¹⁵CH₃ and ¹⁶CH₃), 20.9 (⁷CH₂) ppm. HRMS (ESI, *m/z*): [M + H]⁺ calcd for C₂₁H₃₁N₂O₂, 343.2386; found: 343.2394.

(3*S*, 7*aR*, 11*aR*)-3-Isopropyl-3,6,7,7*a*,8,9,10,11-octahydro-2H-oxazolo[2,3-*j*][1,6]naphthyridin-5-one; Formic Acid (**14**). Compound **1** (655 mg, 1.99 mmol, 1 equiv) was dissolved in methanol (20 mL), and then Pd/C 10% (127 mg, 1.20 mmol, 0.12 mmol, 10

mol %) and ammonium formate (629 mg, 9.97 mmol, 5 equiv) were added. The mixture was refluxed for 30 min. The solution was filtered over celite, and then the filtrate was concentrated under reduced pressure to afford the desired product **14** with a quantitative yield as a white powder. ¹H NMR (300 MHz, CD₂Cl₂): δ 8.44 (brs, 1H), 4.13–3.99 (m, 2H), 3.77 (dd, *J* = 8.3, 5.6 Hz, 1H), 3.35–3.11 (m, 3H), 2.99 (td, *J* = 13.1, 3.2 Hz, 1H), 2.68–2.55 (m, 1H), 2.48–2.20 (m, 2H), 2.10 (td, *J* = 14.4, 4.6 Hz, 1H), 2.01–1.70 (m, 4H), 0.92 (d, *J* = 6.4 Hz, 3H), 0.90 (d, *J* = 6.4 Hz, 3H) ppm. HRMS (ESI, *m/z*): [M + H]⁺ calcd for C₁₃H₂₂N₂O₂, 239.1760; found 239.1759.

General Protocol 2: Alkylation of Compound 14. Compound **14** (1 equiv) was dissolved in MeCN (0.1 N), and then K₂CO₃ (3 equiv) and the appropriate bromide (1–1.5 equiv) and NaI (0–1 equiv) were added. The solution was stirred at room temperature. When the conversion of **14** into the desired product was judged completely by LC/MS or TLC, the solvent was removed under reduced pressure. The residue obtained was dissolved in H₂O and extracted with dichloromethane. The organic layer was dried over MgSO₄, filtered, and concentrated under vacuum to give the crude product, which was purified by flash chromatography column over silica gel using cyclohexane/ethyl acetate (1/0 to 0/1) to afford the corresponding desired lactams.

(3*S*, 7*aR*, 11*aR*)-3-Isopropyl-9-(*p*-tolylmethyl)-2,3,6,7,7*a*,8,10,11-octahydrooxazolo[2,3-*j*][1,6]naphthyridin-5-one (**9**). The product **9** was obtained from 1-(bromomethyl)-4-methyl-benzene using general protocol 2 (yield = 28%), as a white powder. ¹H NMR (300 MHz, CDCl₃): δ 7.19 (d of AB system, *J* = 8.0 Hz, 2H, ^{Ar}CH), 7.11 (d of AB system, *J* = 8.0 Hz, 2H, ^{Ar}CH), 4.12–4.04 (m, 1H, ³CH), 3.97 (dd, *J* = 8.6, 7.6 Hz, 1H, ²CH₂), 3.76 (dd, *J* = 8.6, 6.2 Hz, 1H, ²CH₂), 3.50 (d of AB system, *J* = 13.1 Hz, 1H, ¹²CH₂), 3.36 (d of AB system, *J* = 13.1 Hz, 1H, ¹²CH₂), 2.77–2.62 (m, 2H, ¹⁰CH₂, and ⁸CH₂), 2.62–2.50 (m, 1H, ⁶CH₂), 2.46–2.34 (m, 3H, ⁸CH₂, ⁷CH₂, and ⁶CH₂), 2.30 (s, 3H, ¹⁶CH₃), 2.24–2.13 (m, 1H, ¹⁰CH₂), 2.07–1.88 (m, 2H, ¹³CH, and ¹¹CH₂), 1.84–1.71 (m, 1H, ¹¹CH₂), 1.70–1.54 (m, 2H, ^{7a}CH, and ⁷CH₂), 0.94 (d, *J* = 6.8 Hz, 3H, ¹⁴ or ¹⁵CH₃), 0.89 (d, *J* = 6.8 Hz, 3H, ¹⁴ or ¹⁵CH₃) ppm. ¹³C NMR (75 MHz, CDCl₃): δ 170.3 (⁵CO), 136.7, 135.9 (^{Ar}Cq), 129.0, 128.7 (^{Ar}CH), 92.8 (^{11a}Cq), 66.2 (²CH₂), 62.3 (¹²CH₂), 61.3 (³CH), 54.8 (⁸CH₂), 50.7 (¹⁰CH₂), 40.5 (^{7a}CH), 32.5 (¹³CH), 32.4 (¹¹CH₂), 30.9 (⁶CH₂), 22.0 (⁷CH₂), 21.2 (¹⁶CH₃), 19.9 (¹⁴ or ¹⁵CH₃), 18.7 (¹⁴ or ¹⁵CH₃) ppm. HRMS (ESI, *m/z*): [M + H]⁺ calcd for C₂₁H₃₀N₂O₂, 343.2386; found 343.2398.

(3*S*, 7*aR*, 11*aR*)-3-Isopropyl-9-[(4-methoxyphenyl)methyl]-2,3,6,7,7*a*,8,10,11-octahydrooxazolo[2,3-*j*][1,6]naphthyridin-5-one (**10**). The product **10** was obtained from 1-(bromomethyl)-4-methoxy-benzene using general protocol 2 (yield = 45%), as a colorless oil. ¹H NMR (300 MHz, CDCl₃): δ 7.21 (d of AB system, *J* = 8.6 Hz, 2H, ^{Ar}CH), 6.85 (d of AB system, *J* = 8.6 Hz, 2H, ^{Ar}CH), 4.14–4.03 (m, 1H, ³CH), 3.98 (dd, *J* = 8.6, 7.6 Hz, 1H, ²CH₂), 3.80 (s, 3H, ¹⁶CH₃), 3.79–3.73 (m, 1H, ²CH₂), 3.48 (d of AB system, *J* = 13.0 Hz, 1H, ¹²CH₂), 3.34 (d of AB system, *J* = 13.0 Hz, 1H, ¹²CH₂), 2.76–2.63 (m, 2H, ¹⁰CH₂, and ⁸CH₂), 2.61–2.51 (m, 1H, ⁶CH₂), 2.45–2.28 (m, 3H, ⁸CH₂, ⁷CH₂ and ⁶CH₂), 2.24–2.13 (m, 1H, ¹⁰CH₂), 2.07–1.89 (m, 2H, ¹³CH and ¹¹CH₂), 1.82–1.71 (m, 1H, ¹¹CH₂), 1.70–1.54 (m, 2H, ^{7a}CH and ⁷CH₂), 0.94 (d, *J* = 6.9 Hz, 3H, ¹⁴ or ¹⁵CH₃), 0.90 (d, *J* = 6.8 Hz, 3H, ¹⁴ or ¹⁵CH₃) ppm. ¹³C NMR (75 MHz, CDCl₃): δ 170.3 (⁵CO), 158.8, 130.9 (^{Ar}Cq), 129.9, 113.7 (^{Ar}CH), 92.8 (^{11a}Cq), 66.2 (²CH₂), 61.9 (¹²CH₂), 61.3 (³CH), 55.4 (¹⁶CH₃), 54.7 (⁸CH₂), 50.6 (¹⁰CH₂), 40.4 (^{7a}CH), 32.5 (¹³CH), 32.4 (¹¹CH₂), 30.9 (⁶CH₂), 22.0 (⁷CH₂), 19.9 (¹⁴ or ¹⁵CH₃), 18.7 (¹⁴ or ¹⁵CH₃) ppm. HRMS (ESI, *m/z*): [M + H]⁺ calcd for C₂₁H₃₀N₂O₃, 359.2335; found 359.2314.

(3*S*, 7*aR*, 11*aR*)-9-[(4-Chlorophenyl)methyl]-3-isopropyl-2,3,6,7,7*a*,8,10,11-octahydrooxazolo[2,3-*j*][1,6]naphthyridin-5-one (**11**). The compound **11** was obtained from 1-chloro-4-(chloromethyl)benzene using general protocol 2 (yield = 42%), as a colorless oil. ¹H NMR (300 MHz, CDCl₃): δ 7.30–7.21 (m, 4H, ^{Ar}CH), 4.14–4.05 (m, 1H, ³CH), 3.98 (dd, *J* = 8.6, 7.6 Hz, 1H, ²CH₂), 3.76 (dd, *J* = 8.6, 6.2 Hz, 1H, ²CH₂), 3.49 (d of AB system, *J* = 13.5 Hz, 1H, ¹²CH₂), 3.37 (d of AB system, *J* = 13.5 Hz, 1H, ¹²CH₂), 2.74–2.61 (m, 2H; ¹⁰CH₂ and ⁸CH₂), 2.60–2.52 (m, 1H, ⁶CH₂),

2.50–2.29 (m, 3H, $^8\text{CH}_2$, $^7\text{CH}_2$ and $^6\text{CH}_2$), 2.26–2.15 (m, 1H, $^{10}\text{CH}_2$), 2.08–1.89 (m, 2H, ^{13}CH and $^{11}\text{CH}_2$), 1.84–1.76 (m, 1H, $^{11}\text{CH}_2$), 1.72–1.56 (m, 2H, ^7aCH and $^7\text{CH}_2$), 0.94 (d, $J = 6.8$ Hz, 3H, 14 or $^{15}\text{CH}_3$), 0.89 (d, $J = 6.8$ Hz, 3H, 14 or $^{15}\text{CH}_3$) ppm. ^{13}C NMR (75 MHz, CDCl_3): δ 170.2 (^5CO), 137.5, 132.7 ($^{\text{Ar}}\text{Cq}$), 130.0, 128.5 ($^{\text{Ar}}\text{CH}$), 92.6 ($^{11\text{a}}\text{Cq}$), 66.2 ($^2\text{CH}_2$), 61.8 ($^{12}\text{CH}_2$), 61.3 (^3CH), 54.8 ($^8\text{CH}_2$), 50.7 ($^{10}\text{CH}_2$), 40.4 (^7aCH), 32.4 (^{13}CH), 32.4 ($^{11}\text{CH}_2$), 30.8 ($^6\text{CH}_2$), 22.0 ($^7\text{CH}_2$), 19.9 (14 or $^{15}\text{CH}_3$), 18.7 (14 or $^{15}\text{CH}_3$) ppm. HRMS (ESI, m/z): $[\text{M} + \text{H}]^+$ calcd for $\text{C}_{20}\text{H}_{28}\text{N}_2\text{O}_2\text{Cl}$, 363.1839; found 363.1872.

(3*S*,7*aR*,11*aR*)-3-Isopropyl-9-[[4-(trifluoromethyl)phenyl]methyl]-2,3,6,7,7*a*,8,10,11-octahydrooxazolo[2,3-*j*][1,6]-naphthyridin-5-one (12). The product 12 was obtained from 1-(bromomethyl)-4-(trifluoromethyl)benzene using general protocol 2 (yield = 73%), as a white powder. ^1H NMR (300 MHz, CD_2Cl_2): δ 7.57 (d of AB system, $J = 8.1$ Hz, 2H, $^{\text{Ar}}\text{CH}$), 7.47 (d of AB system, $J = 8.1$ Hz, 2H, $^{\text{Ar}}\text{CH}$), 4.07–3.94 (m, 2H, ^3CH and $^2\text{CH}_2$), 3.75 (dd, $J = 8.0$, 5.7 Hz, 1H, $^2\text{CH}_2$), 3.58 (d of AB system, $J = 13.9$ Hz, 1H, $^{12}\text{CH}_2$), 3.48 (d of AB system, $J = 13.9$ Hz, 1H, $^{12}\text{CH}_2$), 2.73–2.61 (m, 2H, $^{10}\text{CH}_2$ and $^8\text{CH}_2$), 2.57–2.45 (m, 2H, $^8\text{CH}_2$ and $^6\text{CH}_2$), 2.41–2.28 (m, 2H, $^7\text{CH}_2$ and $^6\text{CH}_2$), 2.27–2.18 (m, 1H, $^{10}\text{CH}_2$), 2.03–1.90 (m, 2H, ^{13}CH and $^{11}\text{CH}_2$), 1.82–1.74 (m, 1H, $^{11}\text{CH}_2$), 1.69–1.56 (m, 2H, ^7aCH and $^7\text{CH}_2$), 0.91 (d, $J = 6.8$ Hz, 3H, 14 or $^{15}\text{CH}_3$), 0.88 (d, $J = 6.8$ Hz, 3H, 14 or $^{15}\text{CH}_3$) ppm. ^{13}C NMR (75 MHz, CD_2Cl_2): δ 170.0 (^5CO), 144.0 ($^{\text{Ar}}\text{Cq}$), 129.2 (q, $J = 32.2$ Hz, $^{\text{Ar}}\text{Cq}$), 129.2 ($^{\text{Ar}}\text{CH}$), 125.4 (q, $J = 3.7$ Hz, $^{\text{Ar}}\text{CH}$), 124.8 (q, $J = 272.1$ Hz, $^{\text{CF}_3}\text{Cq}$), 92.7 ($^{11\text{a}}\text{Cq}$), 66.4 ($^2\text{CH}_2$), 62.2 ($^{12}\text{CH}_2$), 61.5 (^3CH), 55.3 ($^8\text{CH}_2$), 51.0 ($^{10}\text{CH}_2$), 40.8 (^7aCH), 32.8 (^{13}CH), 32.6 ($^{11}\text{CH}_2$), 31.2 ($^6\text{CH}_2$), 32.3 ($^7\text{CH}_2$), 19.9 (14 or $^{15}\text{CH}_3$), 18.7 (14 or $^{15}\text{CH}_3$) ppm. LCMS (ESI, m/z): $t_r = 2.83$ min, $[\text{M} + \text{H}]^+ = 397$. HRMS (ESI, m/z): $[\text{M} + \text{H}]^+$ calcd for $\text{C}_{21}\text{H}_{27}\text{N}_2\text{O}_2\text{F}_3$, 397.2103; found 396.2101.

(3*S*,7*aR*,11*aR*)-3-Isopropyl-9-[[4-(trifluoromethoxy)phenyl]methyl]-2,3,6,7,7*a*,8,10,11-octahydrooxazolo[2,3-*j*][1,6]-naphthyridin-5-one (13). The product 13 was obtained from 1-(bromomethyl)-4-(trifluoromethoxy)benzene using general protocol 2 (yield = 77%), as a colorless oil. ^1H NMR (300 MHz, CD_2Cl_2): δ 7.38 (d of AB system, $J = 8.6$ Hz, 2H, $^{\text{Ar}}\text{CH}$), 7.17 (d of AB system, $J = 8.6$ Hz, 2H, $^{\text{Ar}}\text{CH}$), 4.07–3.94 (m, 2H, ^3CH and $^2\text{CH}_2$), 3.75 (dd, $J = 8.0$, 5.7 Hz, 1H, $^2\text{CH}_2$), 3.52 (d of AB system, $J = 13.6$ Hz, 1H, $^{12}\text{CH}_2$), 3.42 (d of AB system, $J = 13.6$ Hz, 1H, $^{12}\text{CH}_2$), 2.74–2.60 (m, 2H, $^{10}\text{CH}_2$ and $^8\text{CH}_2$), 2.58–2.42 (m, 2H, $^8\text{CH}_2$ and $^6\text{CH}_2$), 2.40–2.26 (m, 2H, $^7\text{CH}_2$ and $^6\text{CH}_2$), 2.26–2.14 (m, 1H, $^{10}\text{CH}_2$), 2.04–1.87 (m, 2H, ^{13}CH and $^{11}\text{CH}_2$), 1.83–1.74 (m, 1H, $^{11}\text{CH}_2$), 1.72–1.54 (m, 2H, ^7aCH and $^7\text{CH}_2$), 0.91 (d, $J = 6.7$ Hz, 3H, 14 or $^{15}\text{CH}_3$), 0.88 (d, $J = 6.7$ Hz, 3H, 14 or $^{15}\text{CH}_3$) ppm. ^{13}C NMR (75 MHz, CD_2Cl_2): δ 170.0 (^5CO), 148.5, 138.6 ($^{\text{Ar}}\text{Cq}$), 130.3, 121.1 ($^{\text{Ar}}\text{CH}$), 120.7 (q, $J = 250.1$ Hz, $^{\text{CF}_3}\text{Cq}$), 92.8 ($^{11\text{a}}\text{Cq}$), 66.4 ($^2\text{CH}_2$), 61.9 ($^{12}\text{CH}_2$), 61.6 (^3CH), 55.3 ($^8\text{CH}_2$), 50.9 ($^{10}\text{CH}_2$), 40.8 (^7aCH), 32.8 (^{13}CH), 32.7 ($^{11}\text{CH}_2$), 31.2 ($^6\text{CH}_2$), 32.3 ($^7\text{CH}_2$), 20.0 (14 or $^{15}\text{CH}_3$), 18.8 (14 or $^{15}\text{CH}_3$) ppm. LCMS (ESI, m/z): $t_r = 2.82$ min, $[\text{M} + \text{H}]^+ = 413$. HRMS (ESI, m/z): $[\text{M} + \text{H}]^+$ calcd for $\text{C}_{21}\text{H}_{28}\text{N}_2\text{O}_3\text{F}_3$, 413.2052; found 413.2056.

(3*S*,7*aR*,11*aR*)-3-Isopropyl-9-[[6-(trifluoromethyl)-3-pyridyl]methyl]-2,3,6,7,7*a*,8,10,11-octahydrooxazolo[2,3-*j*][1,6]-naphthyridin-5-one (13). To a solution of compound 14 (500 mg, 1.76 mmol, 1 equiv) in dichloroethane (4 mL) were added 6-(trifluoromethyl)pyridine-3-carbaldehyde (1.1 g, 6.29 mmol, 3.6 equiv), titanium isopropoxide (937 μL , 3.15 mmol, 1.8 equiv), and $\text{NaBH}(\text{OAc})_3$ (1.33 g, 6.29 mmol, 3.6 equiv). The mixture was stirred at room temperature overnight. The solvent was removed under vacuum, and the mixture was then taken up in CH_2Cl_2 and washed with a saturated aqueous solution of Na_2CO_3 . The organic layer was dried over magnesium sulfate, filtered, and concentrated under vacuum. The product was purified by flash chromatography column over silica gel using cyclohexane/ethyl acetate (1/0 to 0/1) to afford the desired product 13 (493 mg, 71%) as a white powder. ^1H NMR (300 MHz, CDCl_3): δ 8.66 (brs, 1H, $^{\text{Ar}}\text{CH}$), 7.85 (dd, $J = 8.0$, 1.3 Hz, 1H, $^{\text{Ar}}\text{CH}$), 7.64 (d, $J = 8.0$ Hz, 1H, $^{\text{Ar}}\text{CH}$), 4.14–4.06 (m, 1H, ^3CH), 3.99 (dd, $J = 8.5$, 8.0 Hz, 1H, $^2\text{CH}_2$), 3.78 (dd, $J = 8.5$, 6.2 Hz, 1H, $^2\text{CH}_2$), 3.62 (d of AB system, $J = 14.1$ Hz, 1H, $^{12}\text{CH}_2$), 3.52 (d of AB

system, $J = 14.1$ Hz, 1H, $^{12}\text{CH}_2$), 2.75–2.52 (m, 4H, $^{10}\text{CH}_2$, $^8\text{CH}_2$ and $^6\text{CH}_2$), 2.48–2.25 (m, 3H, $^{10}\text{CH}_2$, $^7\text{CH}_2$ and $^6\text{CH}_2$), 2.07–1.91 (m, 2H, ^{13}CH and $^{11}\text{CH}_2$), 1.85–1.77 (m, 1H, $^{11}\text{CH}_2$), 1.75–1.59 (m, 2H, ^7aCH and $^7\text{CH}_2$), 0.95 (d, $J = 6.8$ Hz, 3H, 14 or $^{15}\text{CH}_3$), 0.91 (d, $J = 6.8$ Hz, 3H, 14 or $^{15}\text{CH}_3$) ppm. ^{13}C NMR (75 MHz, CDCl_3): δ 170.1 (^5CO), 129.2 ($^{\text{Ar}}\text{CH}$), 147.2 (q, $J = 33.5$ Hz, $^{\text{Ar}}\text{Cq}$), 137.9 ($^{\text{Ar}}\text{Cq}$), 137.5 ($^{\text{Ar}}\text{CH}$), 121.5 (q, $J = 272.0$ Hz, $^{\text{CF}_3}\text{Cq}$), 120.3 (q, $J = 3.7$ Hz, $^{\text{Ar}}\text{CH}$), 92.3 ($^{11\text{a}}\text{Cq}$), 66.3 ($^2\text{CH}_2$), 61.3 ($^{12}\text{CH}_2$), 59.4 (^3CH), 55.0 ($^8\text{CH}_2$), 50.8 ($^{10}\text{CH}_2$), 40.3 (^7aCH), 32.4 (^{13}CH), 32.3 ($^{11}\text{CH}_2$), 30.7 ($^6\text{CH}_2$), 21.9 ($^7\text{CH}_2$), 19.9, 18.7 (14 and $^{15}\text{CH}_3$) ppm. LCMS (ESI, m/z): $t_r = 2.77$ min, $[\text{M} + \text{H}]^+ = 398$. HRMS (ESI, m/z): $[\text{M} + \text{H}]^+$ calcd for $\text{C}_{20}\text{H}_{27}\text{N}_3\text{O}_2\text{F}_3$, 398.2055; found 398.2044.

ASSOCIATED CONTENT

Supporting Information

The Supporting Information is available free of charge at <https://pubs.acs.org/doi/10.1021/acs.jmedchem.2c01493>.

All biological, ADME, and X-ray diffraction methods, supplementary tables and figures, ^1H and ^{13}C NMR spectra, and HRMS spectra of all synthesized compounds as well as 2-D NMR and HPLC-MS traces for lead compounds (PDF)

Compound SMILES and biological data (CSV)

AUTHOR INFORMATION

Corresponding Authors

Nicolas Willand – Univ. Lille, Inserm, Institut Pasteur de Lille, U1177 - Drugs and Molecules for Living Systems, F-59000 Lille, France; Email: nicolas.willand@univ-lille.fr

Baptiste Villemagne – Univ. Lille, Inserm, Institut Pasteur de Lille, U1177 - Drugs and Molecules for Living Systems, F-59000 Lille, France; orcid.org/0000-0002-8416-5253; Email: baptiste.villemagne@univ-lille.fr

Ruben C. Hartkoorn – Univ. Lille, CNRS, Inserm, CHU Lille, Institut Pasteur Lille, U1019 - UMR 9017 - CIIL - Center for Infection and Immunity of Lille, F-59000 Lille, France; orcid.org/0000-0001-7315-1553; Email: ruben.hartkoorn@inserm.fr

Authors

Sushovan Dam – Univ. Lille, CNRS, Inserm, CHU Lille, Institut Pasteur Lille, U1019 - UMR 9017 - CIIL - Center for Infection and Immunity of Lille, F-59000 Lille, France

Salia Tangara – Univ. Lille, Inserm, Institut Pasteur de Lille, U1177 - Drugs and Molecules for Living Systems, F-59000 Lille, France

Claire Hamela – Centre National de la Recherche Scientifique, Institut de Recherche en Infectiologie de Montpellier, UMR 9004, Université de Montpellier, 34293 Montpellier, France

Theo Hattabi – Univ. Lille, Inserm, Institut Pasteur de Lille, U1177 - Drugs and Molecules for Living Systems, F-59000 Lille, France

Léo Faïon – Univ. Lille, Inserm, Institut Pasteur de Lille, U1177 - Drugs and Molecules for Living Systems, F-59000 Lille, France

Paul Carre – Univ. Lille, CNRS, Inserm, CHU Lille, Institut Pasteur Lille, U1019 - UMR 9017 - CIIL - Center for Infection and Immunity of Lille, F-59000 Lille, France

Rudy Antoine – Univ. Lille, CNRS, Inserm, CHU Lille, Institut Pasteur Lille, U1019 - UMR 9017 - CIIL - Center for Infection and Immunity of Lille, F-59000 Lille, France

Adrien Herledan – Univ. Lille, Inserm, Institut Pasteur de Lille, U1177 - Drugs and Molecules for Living Systems, F-59000 Lille, France

Florence Leroux – Univ. Lille, Inserm, Institut Pasteur de Lille, U1177 - Drugs and Molecules for Living Systems, F-59000 Lille, France

Catherine Piveteau – Univ. Lille, Inserm, Institut Pasteur de Lille, U1177 - Drugs and Molecules for Living Systems, F-59000 Lille, France

Maxime Eveque – Univ. Lille, Inserm, Institut Pasteur de Lille, U1177 - Drugs and Molecules for Living Systems, F-59000 Lille, France

Marion Flipo – Univ. Lille, Inserm, Institut Pasteur de Lille, U1177 - Drugs and Molecules for Living Systems, F-59000 Lille, France

Benoit Deprez – Univ. Lille, Inserm, Institut Pasteur de Lille, U1177 - Drugs and Molecules for Living Systems, F-59000 Lille, France

Laurent Kremer – Centre National de la Recherche Scientifique, Institut de Recherche en Infectiologie de Montpellier, UMR 9004, Université de Montpellier, 34293 Montpellier, France; INSERM, IRIM, 34293 Montpellier, France; orcid.org/0000-0002-6604-4458

Complete contact information is available at: <https://pubs.acs.org/10.1021/acs.jmedchem.2c01493>

Author Contributions

S.D., S.T., C.H., T.A., L.F., L.K., N.W., B.V., and R.C.H. designed experiments. N.W. and B.D. designed, generated, and compiled the screened chemical library. S.T., T.A., L.F., M.F., B.D., N.W., and B.V. designed, synthesized, and characterized TriSLa analogues. A.H., F.L., N.W., and R.C.H. performed the chemical library screening. Selection of TriSLa-resistant isolates was performed by SD and RCH. Metabolic stability was determined by C.P., M.E., and B.V. Phys-chem properties were determined by C.P., M.E., and B.V. Antibacterial In vitro profiling of TriSLa compounds was performed by S.D. and R.C.H. Biochemical validation was performed by S.D., P.C., and R.C.H. In vivo efficacy studies on *M. marinum*-infected zebrafish and analysis were performed by C.H. and L.K. S.D., S.T., C.H., L.F., M.F., B.D., L.K., N.W., B.V., and R.C.H. wrote the paper. N.W., B.V., and R.C.H. obtained funding for this work. S.D., S.T., and C.H. contributed equally.

Notes

The authors declare the following competing financial interest(s): SD, ST, TA, LF, MF, BD, NW, BV and RCH, are inventors on patent application covering the TriSLa molecules described in this manuscript. The remaining authors declare no competing interests.

Atomic coordinates and structure factors reported in this paper (crystal structure of **BDM44410**, **1**) have been deposited in the Cambridge Structural Database under accession number CCDC 2143694. Whole genome sequencing data (fastq files) for parental and **BDM44410** (**1**) resistant H37Rv isolates (RC14.2, RC28.1) have been deposited at NCBI (BioProject ID: PRJNA808942).

ACKNOWLEDGMENTS

We thank F. Capet and P. Roussel from the X-ray platform of Chevrel Institute (FR CNRS 2638), for supporting data collection and solving the x-ray crystal structure. We thank V. Landry (U1177- Drugs and Molecules for Living Systems) for cytotoxicity experiments. We thank BLS-3 Facility staff (N. Vandenabeele, R. Prath, and S. Marin) at the Institut Pasteur de Lille for technical support. We thank E. Anoz Carbonell for

unbiased MIC analysis. We are grateful to P. Richard and M. Plays for zebrafish husbandry. This research was financially cofunded by NL4Tb, Atip-Avenir, SMART-Lab, and CPER grants. The NL4Tb grant was funded by the French National Research Agency (ANR-19-CE18-0034-01). The SMART-Lab grant was funded by European Union under the European Regional Development Fund (ERDF), by the Hauts De France Regional Council (Contract n°NP0020070), and by I-Site ULNE (ANR-16-IDEX-0004 ULNE). The CPER grants were funded by European Union under the European Regional Development Fund (ERDF) and by the Hauts de France regional Council (contract n°20002842 and contract n°18006176), the MEL (contract n°2017_ESR_14 and contract_2020_ESR_06), and the French State (contract n°2018-R3-CTRL-Phase2 and contract n°2020-R3-CTRL_IPL_Phase4). The compound management and physicochemical/ADME property measurement were supported by ChemBio-France through the ARIADNE-ADME platform (Lille, France). We thank the NMR platform of the faculty of pharmacy, Lille University for the use of the 300 MHz NMR facilities, funded by the Région Hauts-De-France, the ministère de la jeunesse de l'éducation Nationale et de la Recherche (MJENR) and the fonds Européens de développement Régional (FEDER).

ABBREVIATIONS

BDQ, bedaquiline; cfu, colony forming unit; dpi, days post-infection; FPC, fluorescent pixel count; hpf, hours post-fertilization; INH, isoniazid; MBP, maltose-binding protein; MDR, multidrug resistant; *Mtb*, *Mycobacterium tuberculosis*; REMA, resazurin microtiter assay; RIF, rifampicin; XDR, extensively drug resistant

REFERENCES

- (1) World Health Organization. *Global Tuberculosis Report 2021*: Geneva, 2021.
- (2) Connolly, L. E.; Edelstein, P. H.; Ramakrishnan, L. Why Is Long-Term Therapy Required to Cure Tuberculosis? *PLoS Med.* **2007**, *4*, No. e120.
- (3) World Health Organization. *Global Tuberculosis Report 2020*: Geneva, 2020.
- (4) World Health Organization. *Global Priority List Of Antibiotic-Resistant Bacteria To Guide Research, Discovery And Development Of New Antibiotics*, 2017.
- (5) Palomino, J. C.; Martin, A. TMC207 Becomes Bedaquiline, a New Anti-TB Drug. *Future Microbiol.* **2013**, *8*, 1071–1080.
- (6) Ryan, N. J.; Lo, J. H. Delamanid: First Global Approval. *Drugs* **2014**, *74*, 1041–1045.
- (7) Keam, S. J. Pretomanid: First Approval. *Drugs* **2019**, *79*, 1797–1803.
- (8) Tiberi, S.; du Plessis, N.; Walzl, G.; Vjecha, M. J.; Rao, M.; Ntoumi, F.; Mfinanga, S.; Kapata, N.; Mwaba, P.; McHugh, T. D.; Ippolito, G.; Migliori, G. B.; Maeurer, M. J.; Zumla, A. Tuberculosis: Progress and Advances in Development of New Drugs, Treatment Regimens, and Host-Directed Therapies. *Lancet Infect. Dis.* **2018**, *18*, e183–e198.
- (9) Tornheim, J. A.; Dooley, K. E. The Global Landscape of Tuberculosis Therapeutics. *Annu. Rev. Med.* **2019**, *70*, 105–120.
- (10) Libardo, M. D. J.; Boshoff, H. I.; Barry, C. E. The Present State of the Tuberculosis Drug Development Pipeline. *Curr. Opin. Pharmacol.* **2018**, *42*, 81–94.
- (11) Mikušová, K.; Ekins, S. Learning from the Past for TB Drug Discovery in the Future. *Drug Discovery Today* **2017**, *22*, 534–545.
- (12) Ballell, L.; Bates, R. H.; Young, R. J.; Alvarez-Gomez, D.; Alvarez-Ruiz, E.; Barroso, V.; Blanco, D.; Crespo, B.; Escibano, J.;

- González, R.; Lozano, S.; Huss, S.; Santos-Villarejo, A.; Martín-Plaza, J. J.; Mendoza, A.; Rebollo-Lopez, M. J.; Remuñán-Blanco, M.; Lavandera, J. L.; Pérez-Herran, E.; Gamo-Benito, F. J.; García-Bustos, J. F.; Barros, D.; Castro, J. P.; Cammack, N. Fueling Open-Source Drug Discovery: 177 Small-Molecule Leads against Tuberculosis. *ChemMedChem* **2013**, *8*, 313–321.
- (13) Kumar, A.; Zhang, K. Y. J. Advances in the Development of Shape Similarity Methods and Their Application in Drug Discovery. *Front. Chem.* **2018**, *6*, 1–21.
- (14) Deprez-Poulain, R.; Willand, N.; Boutillon, C.; Nowogrocki, G.; Azaroual, N.; Deprez, B. A Simple Reaction to Produce Small Structurally Complex and Diverse Molecules. *Tetrahedron Lett.* **2004**, *45*, 5287–5290.
- (15) Willand, N.; Beghyn, T.; Nowogrocki, G.; Gesquiere, J.-C.; Deprez, B. Synthesis and Structural Studies of a Novel Scaffold for Drug Discovery: A 4,5-Dihydro-3H-Spiro[1,5-Benzoxazepine-2,4'-Piperidine]. *Tetrahedron Lett.* **2004**, *45*, 1051–1054.
- (16) Willand, N.; Folléas, B.; Boutillon, C.; Verbraeken, L.; Gesquiere, J.-C.; Tartar, A.; Deprez, B. Efficient, Two-Step Synthesis of N-Substituted Nortropinone Derivatives. *Tetrahedron Lett.* **2007**, *48*, 5007–5011.
- (17) Malaquin, S.; Jida, M.; Courtin, J.; Laconde, G.; Willand, N.; Deprez, B.; Deprez-Poulain, R. Water-Based Conditions for the Microscale Parallel Synthesis of Bicyclic Lactams. *Tetrahedron Lett.* **2013**, *54*, 562–567.
- (18) Tran, N. C.; Dhondt, H.; Flipo, M.; Deprez, B.; Willand, N. Synthesis of Functionalized 2-Isoxazolines as Three-Dimensional Fragments for Fragment-Based Drug Discovery. *Tetrahedron Lett.* **2015**, *56*, 4119–4123.
- (19) Prevet, H.; Flipo, M.; Roussel, P.; Deprez, B.; Willand, N. Microwave-Assisted Synthesis of Functionalized Spirohydantoins as 3-D Privileged Fragments for Scouting the Chemical Space. *Tetrahedron Lett.* **2016**, *57*, 2888–2894.
- (20) Blondiaux, N.; Moune, M.; Desroses, M.; Frita, R.; Flipo, M.; Mathys, V.; Soetaert, K.; Kiass, M.; Delorme, V.; Djaout, K.; Trebosc, V.; Kemmer, C.; Wintjens, R.; Wohlkönig, A.; Antoine, R.; Huot, L.; Hot, D.; Coscolla, M.; Feldmann, J.; Gagneux, S.; Loch, C.; Brodin, P.; Gitzinger, M.; Déprez, B.; Willand, N.; Baulard, A. R. Reversion of Antibiotic Resistance in Mycobacterium Tuberculosis by Spiroisoxazoline SMART-420. *Science* **2017**, *355*, 1206–1211.
- (21) Prevet, H.; Moune, M.; Tanina, A.; Kemmer, C.; Herledan, A.; Frita, R.; Wohlkönig, A.; Bourotte, M.; Villemagne, B.; Leroux, F.; Gitzinger, M.; Baulard, A. R.; Déprez, B.; Wintjens, R.; Willand, N.; Flipo, M. A Fragment-Based Approach towards the Discovery of N-Substituted Tropinones as Inhibitors of Mycobacterium Tuberculosis Transcriptional Regulator EthR2. *Eur. J. Med. Chem.* **2019**, *167*, 426–438.
- (22) von Korff, M.; Sander, T. About Complexity and Self-Similarity of Chemical Structures in Drug Discovery. In *Chaos and Complex Systems*; Springer, Berlin, Heidelberg: Berlin, Heidelberg, 2013; pp 301–306.
- (23) Sander, T.; Freyss, J.; von Korff, M.; Rufener, C. DataWarrior: An Open-Source Program For Chemistry Aware Data Visualization And Analysis. *J. Chem. Inf. Model.* **2015**, *55*, 460–473.
- (24) Koul, A.; Vranckx, L.; Dhar, N.; Göhlmann, H. W. H.; Özdemir, E.; Neefs, J.-M.; Schulz, M.; Lu, P.; Mørtz, E.; McKinney, J. D.; Andries, K.; Bald, D. Delayed Bactericidal Response of Mycobacterium Tuberculosis to Bedaquiline Involves Remodelling of Bacterial Metabolism. *Nat. Commun.* **2014**, *5*, 3369.
- (25) Vocat, A.; Hartkoorn, R. C.; Lechartier, B.; Zhang, M.; Dhar, N.; Cole, S. T.; Sala, C. Bioluminescence for Assessing Drug Potency against Nonreplicating Mycobacterium Tuberculosis. *Antimicrob. Agents Chemother.* **2015**, *59*, 4012–4019.
- (26) Zhang, M.; Sala, C.; Hartkoorn, R. C.; Dhar, N.; Mendoza-Losana, A.; Cole, S. T. Streptomycin-Starved Mycobacterium Tuberculosis 18b, a Drug Discovery Tool for Latent Tuberculosis. *Antimicrob. Agents Chemother.* **2012**, *56*, 5782–5789.
- (27) Varadi, M.; Anyango, S.; Deshpande, M.; Nair, S.; Natassia, C.; Yordanova, G.; Yuan, D.; Stroe, O.; Wood, G.; Laydon, A.; Židek, A.; Green, T.; Tunyasuvunakool, K.; Petersen, S.; Jumper, J.; Clancy, E.; Green, R.; Vora, A.; Lutfi, M.; Figurnov, M.; Cowie, A.; Hobbs, N.; Kohli, P.; Kleywegt, G.; Birney, E.; Hassabis, D.; Velankar, S. AlphaFold Protein Structure Database: Massively Expanding the Structural Coverage of Protein-Sequence Space with High-Accuracy Models. *Nucleic Acids Res.* **2022**, *50*, D439–D444.
- (28) Jumper, J.; Evans, R.; Pritzel, A.; Green, T.; Figurnov, M.; Ronneberger, O.; Tunyasuvunakool, K.; Bates, R.; Židek, A.; Potapenko, A.; Bridgland, A.; Meyer, C.; Kohl, S. A. A.; Ballard, A. J.; Cowie, A.; Romera-Paredes, B.; Nikolov, S.; Jain, R.; Adler, J.; Back, T.; Petersen, S.; Reiman, D.; Clancy, E.; Zielinski, M.; Steinegger, M.; Pacholska, M.; Berghammer, T.; Bodenstein, S.; Silver, D.; Vinyals, O.; Senior, A. W.; Kavukcuoglu, K.; Kohli, P.; Hassabis, D. Highly Accurate Protein Structure Prediction with AlphaFold. *Nature* **2021**, *596*, 583–589.
- (29) Murugesan, D.; Ray, P. C.; Bayliss, T.; Prosser, G. A.; Harrison, J. R.; Green, K.; Soares de Melo, C.; Feng, T.-S.; Street, L. J.; Chibale, K.; Warner, D. F.; Mizrahi, V.; Epemolu, O.; Scullion, P.; Ellis, L.; Riley, J.; Shishikura, Y.; Ferguson, L.; Osuna-Cabello, M.; Read, K. D.; Green, S. R.; Lamprecht, D. A.; Finin, P. M.; Steyn, A. J. C.; Joerger, T. R.; Sacchettini, J.; Rhee, K. Y.; Arora, K.; Barry, C. E.; Wyatt, P. G.; Boshoff, H. I. M. 2-Mercapto-Quinazolinones as Inhibitors of Type II NADH Dehydrogenase and Mycobacterium Tuberculosis: Structure–Activity Relationships, Mechanism of Action and Absorption, Distribution, Metabolism, and Excretion Characterization. *ACS Infect. Dis.* **2018**, *4*, 954–969.
- (30) Vilchère, C.; Weinrick, B.; Leung, L. W.; Jacobs, W. R. Plasticity of Mycobacterium Tuberculosis NADH Dehydrogenases and Their Role in Virulence. *Proc. Natl. Acad. Sci. U. S. A.* **2018**, *115*, 1599–1604.
- (31) Beites, T.; O'Brien, K.; Tiwari, D.; Engelhart, C. A.; Walters, S.; Andrews, J.; Yang, H.-J.; Sutphen, M. L.; Weiner, D. M.; Dayao, E. K.; Zimmerman, M.; Prideaux, B.; Desai, P. V.; Masquelin, T.; Via, L. E.; Dartois, V.; Boshoff, H. I.; Barry, C. E.; Ehrst, S.; Schnappinger, D. Plasticity of the Mycobacterium Tuberculosis Respiratory Chain and Its Impact on Tuberculosis Drug Development. *Nat. Commun.* **2019**, *10*, 4970.
- (32) Miesel, L.; Weisbrod, T. R.; Marcinkeviciene, J. A.; Bittman, R.; Jacobs, W. R. NADH Dehydrogenase Defects Confer Isoniazid Resistance and Conditional Lethality in Mycobacterium Smegmatis. *J. Bacteriol.* **1998**, *180*, 2459–2467.
- (33) Harbut, M. B.; Yang, B.; Liu, R.; Yano, T.; Vilchère, C.; Cheng, B.; Lockner, J.; Guo, H.; Yu, C.; Franzblau, S. G.; Petrassi, H. M.; Jacobs, W. R.; Rubin, H.; Chatterjee, A. K.; Wang, F. Small Molecules Targeting Mycobacterium Tuberculosis Type II NADH Dehydrogenase Exhibit Antimycobacterial Activity. *Angew. Chem., Int. Ed.* **2018**, *57*, 3478–3482.
- (34) Takaki, K.; Cosma, C. L.; Troll, M. A.; Ramakrishnan, L. An In Vivo Platform for Rapid High-Throughput Antitubercular Drug Discovery. *Cell Rep.* **2012**, *2*, 175–184.
- (35) Clay, H.; Volkman, H. E.; Ramakrishnan, L. Tumor Necrosis Factor Signaling Mediates Resistance to Mycobacteria by Inhibiting Bacterial Growth and Macrophage Death. *Immunity* **2008**, *29*, 283–294.
- (36) Volkman, H. E.; Clay, H.; Beery, D.; Chang, J. C. W.; Sherman, D. R.; Ramakrishnan, L. Tuberculous Granuloma Formation Is Enhanced by a Mycobacterium Virulence Determinant. *PLoS Biol.* **2004**, *2*, No. e367.
- (37) Alibaud, L.; Rombouts, Y.; Trivelli, X.; Burguière, A.; Cirillo, S. L. G.; Cirillo, J. D.; Dubremetz, J.-F.; Guérardel, Y.; Lutfalla, G.; Kremer, L. A Mycobacterium Marinum TesA Mutant Defective for Major Cell Wall-Associated Lipids Is Highly Attenuated in Dictyostelium Discoideum and Zebrafish Embryos. *Mol. Microbiol.* **2011**, *80*, 919–934.
- (38) Beghyn, T.; Deprez-Poulain, R.; Willand, N.; Folléas, B.; Deprez, B. Natural Compounds: Leads or Ideas? Bioinspired Molecules for Drug Discovery. *Chem. Biol. Drug Des.* **2008**, *72*, 3–15.
- (39) Lee, M.-L.; Schneider, G. Scaffold Architecture and Pharmacophoric Properties of Natural Products and Trade Drugs:

Application in the Design of Natural Product-Based Combinatorial Libraries. *J. Comb. Chem.* **2001**, *3*, 284–289.

(40) Henkel, T.; Brunne, R. M.; Müller, H.; Reichel, F. Statistical Investigation into the Structural Complementarity of Natural Products and Synthetic Compounds. *Angew. Chem., Int. Ed.* **1999**, *38*, 643–647.

(41) Hong, W. D.; Gibbons, P. D.; Leung, S. C.; Amewu, R.; Stocks, P. A.; Stachulski, A.; Horta, P.; Cristiano, M. L. S.; Shone, A. E.; Moss, D.; Ardrey, A.; Sharma, R.; Warman, A. J.; Bedingfield, P. T. P.; Fisher, N. E.; Aljayyousi, G.; Mead, S.; Caws, M.; Berry, N. G.; Ward, S. A.; Biagini, G. A.; O'Neill, P. M.; Nixon, G. L. Rational Design, Synthesis, and Biological Evaluation of Heterocyclic Quinolones Targeting the Respiratory Chain of Mycobacterium Tuberculosis. *J. Med. Chem.* **2017**, *60*, 3703–3726.

(42) Heikal, A.; Nakatani, Y.; Jiao, W.; Wilson, C.; Rennison, D.; Weimar, M. R.; Parker, E. J.; Brimble, M. A.; Cook, G. M. 'Tethering' Fragment-Based Drug Discovery to Identify Inhibitors of the Essential Respiratory Membrane Protein Type II NADH Dehydrogenase. *Bioorg. Med. Chem. Lett.* **2018**, *28*, 2239–2243.

(43) Shirude, P. S.; Paul, B.; Roy Choudhury, N.; Kedari, C.; Bandodkar, B.; Ugarkar, B. G. Quinoliny Pyrimidines: Potent Inhibitors of NDH-2 as a Novel Class of Anti-TB Agents. *ACS Med. Chem. Lett.* **2012**, *3*, 736–740.

(44) Lu, L.; Åkerbladh, L.; Ahmad, S.; Konda, V.; Cao, S.; Vocat, A.; Maes, L.; Cole, S. T.; Hughes, D.; Larhed, M.; Brandt, P.; Karlén, A.; Mowbray, S. L. Synthesis and In Vitro Biological Evaluation of Quinoliny Pyrimidines Targeting Type II NADH-Dehydrogenase (NDH-2). *ACS Infect. Dis.* **2022**, *8*, 482.

(45) Johansen, M. D.; Kasparian, J. A.; Hortle, E.; Britton, W. J.; Purdie, A. C.; Oehlers, S. H. Mycobacterium Marinum Infection Drives Foam Cell Differentiation in Zebrafish Infection Models. *Dev. Comp. Immunol.* **2018**, *88*, 169–172.